RSC Advances

PAPER

View Article Online
View Journal | View Issue

Cite this: *RSC Adv.*, 2025, **15**, 35941

Development of carboximidamide small molecule nanogels as potent antimicrobial functional drug delivery systems

Basmah Almohaywi,[a] Mohammed H. Elkomy,[bc] Mohamed A. M. Ali,[d] Ahmed K. B. Aljohani,[e] Mohammed S. Abdulrahman,[f] Mohamed M. Elsebaie,*[g] Alaa M. Alhammad,[h] Khadijah A. Aytah,[h] Seba M. Alshehri,[h] Elaaf O. Alharbi,[i] Rama R. Alharbi[h] and Hany E. A. Ahmed*[g]

The escalating threat of multidrug-resistant (MDR) bacterial infections necessitates innovative antimicrobial strategies with enhanced potency, selectivity, and pharmacokinetic profiles. In this study, chitosan/polyvinyl pyrrolidone (Cs/PVP) nanogels were developed to encapsulate hydrophobic scaffolds (phenyltriazole, phenylthiazole, and phenylguanidine derivatives) to improve solubility, stability, and antimicrobial efficacy. The nanogels exhibited nanoscale dimensions (35–320 nm), uniform spherical morphology, and good colloidal stability. Antimicrobial evaluation revealed significant fold potentiation of activity, with minimal inhibitory concentration (MIC) values reduced up to 64-fold against Gram-positive bacteria, particularly methicillin-resistant *Staphylococcus aureus* (MRSA) and *S. epidermidis*. DNA gyrase inhibition assays confirmed enhanced enzyme targeting, with TRZS-nanogels achieving an IC_{50} of 4.44 μg mL^{-1}, representing a 5.7-fold improvement compared to the free compound. Furthermore, nanogels significantly inhibited biofilm formation, achieving up to 79% inhibition in MRSA and 69% in *Pseudomonas aeruginosa*. Cytotoxicity studies on human fibroblast cells demonstrated high biocompatibility, with cell viability maintained above 85% at therapeutic concentrations. These findings highlight Cs/PVP nanogels as promising drug delivery systems with dual antibacterial mechanisms, offering improved potency, safety, and potential clinical application against MDR infections.

Received 17th July 2025
Accepted 21st September 2025

DOI: 10.1039/d5ra05150a

rsc.li/rsc-advances

1. Introduction

The global rise of multidrug-resistant (MDR) bacterial infections, exemplified by pathogens such as methicillin-resistant *Staphylococcus aureus* (MRSA), poses a formidable challenge to public health, exacerbated by the overuse of antibiotics since their discovery in 1928.[1,2] The increasing prevalence of hospital-acquired (HA-MRSA) and community-acquired (CA-MRSA) strains, coupled with their resistance to conventional therapies, underscores the urgent need for innovative antimicrobial strategies.[3,4] Non-antibiotic agents include Antimicrobial Peptides (AMPs), silver nanoparticles, metal oxides, peptoids, and polymers: these have shown some promise in physically disrupting bacterial membranes or in inducing ROS, thereby circumventing traditional resistance mechanisms.[5–7] They are only effective when adminstered through efficient delivery systems to avoid bacterial resistance, such as efflux pumps and degrading enzymes.[8,9] Polymeric nanomaterials, such as dendrimers, micelles, and nanogels, offer significant potential due to their tunable chemical structures, controlled release profiles, and ability to facilitate targeted delivery.[10] In addition to therapeutic applications, antimicrobial coatings for medical devices, textiles, food packaging, marine equipment and water purification systems are also important in addressing the risks associated with biofilms.[11,12] The supercell interactions and internalizing nature of nanogels, merger products of nanoparticles and hydrogels, their size and charge tunability, and

[a]*Department of Pharmaceutical Chemistry, College of Pharmacy, King Khalid University, Abha 61421, Saudi Arabia*
[b]*Department of Pharmaceutics, College of Pharmacy, Jouf University, Sakaka, Aljouf 72341, Saudi Arabia*
[c]*Center for Health Research and Innovations, Deanship of Graduate Studies and Scientific Research, Jouf University, Sakaka 72388, Saudi Arabia*
[d]*Department of Biology, College of Science, Imam Mohammad Ibn Saud Islamic University (IMSIU), Riyadh 11623, Saudi Arabia*
[e]*Pharmacognosy and Pharmaceutical Chemistry Department, Pharmacy College, Taibah University, Al-Madinah Al-Munawarah 42353, Saudi Arabia. E-mail: Akjohani@taibahu.edu.sa*
[f]*Microbiology and Immunology Department, Faculty of Pharmacy, Al-Azhar University, Nasr City 11884, Cairo, Egypt*
[g]*Pharmaceutical Organic Chemistry Department, Faculty of Pharmacy, Al-Azhar University, Nasr City 11884, Cairo, Egypt. E-mail: m.elsebaei@azhar.edu.eg; heahmad@azhar.edu.eg*
[h]*Pharmcy Student, Pharmacy College, Taibah University, Al-Madinah Al-Munawarah 42353, Saudi Arabia*
[i]*Pharmacy Graduate, Pharmacy College, Taibah University, Al-Madinah Al-Munawarah 42353, Saudi Arabia*

their design towards responsiveness to environmental stimuli make them ideal for use in applications such as antimicrobial, antifouling, and on-demand drug delivery.[13]

Many researchers are integrating nanomaterials such as liposomes, polymers and biomimetic membranes, into rapid diagnostic and delivery systems to combat antibiotic resistance and improve diagnostic sensitivity.[14–17] To date, methicillin-resistant MRSA strains, such as hospital acquired (HA)-MRSA and community acquired (CA)-MRSA, have been the most severe public health challenge.[18–21]

In recent years, different chemical scaffolds have been published, including pyranopyrazole, phenylthiazole, and phenyltriazole, which have been shown to have potent antibacterial and antifungal activity.[16,22–27] As the data showed, the prominent antibacterial selectivity affected the microbial biological targets.

Recent studies have identified potent antibacterial and antifungal properties in chemical scaffolds such as pyranopyrazole, phenylthiazole, and phenyltriazole.[28–33] However, clinical translation remains limited due to poor water solubility, narrow spectrum activity, and insufficient penetration into microbial cells and biofilms.[22,23,34–39] These problems hamper their ability to effectively combat resistant and polymicrobial infections. To overcome these problems, the study proposes a new strategy, the development of a delivery system based on nanogels using chitosan/polyvinylpyrrolidone (Cs/PVP). Cs/PVP nanogels offer biocompatibility, improved solubility of hydrophobic drugs, and enhanced penetration and sustained release at the site of infection. Incorporating these scaffolds into the Cs/PVP nanogel matrix can enhance their pharmacological properties and broaden their antimicrobial efficacy, offering a promising approach against antibiotic-resistant pathogens.

It was explored that the expanded application of hydrogel-based nanocapillaries in bacterial research through pH monitoring could affect bacterial growth.[40] In this sense, we have formulated nanogels of chitosan/polyvinyl pyrrolidone (Cs/PVP) that can bind certain hydrophobic antibacterial compounds, including phenylthiazole, phenyltriazole, and phenylguanidine, for evaluation against both Gram-positive and Gram-negative bacteria.

As a continuation of our previously published work on the antimicrobial efficacy of phenyltriazole and phenylthiazole scaffolds against *Staphylococcus aureus* (MRSA) and fungal pathogens,[28,41,42] the current study aims to enhance their therapeutic potential through nanogel-based formulation. Given the promising *in vitro* results of these novel compounds, this research focuses on encapsulating selected derivatives into biocompatible chitosan/polyvinyl pyrrolidone (Cs/PVP) nanogels to improve their solubility, targeted delivery, and overall pharmacokinetic behavior. To address these limitations, this study aims to develop a chitosan/polyvinyl pyrrolidone (Cs/PVP) nanogel-based delivery system to enhance the solubility, targeted delivery, and pharmacokinetic properties of hydrophobic antibacterial agents, specifically phenylthiazole, phenyltriazole, and phenylguanidine. By encapsulating these scaffolds into biocompatible Cs/PVP nanogels, we seek to improve their antimicrobial efficacy against MDR pathogens through a dual-action mechanism targeting DNA gyrase and bacterial membrane disruption. Additionally, we aim to evaluate the nanogels' physicochemical properties, biocompatibility, and anti-biofilm activity, establishing a robust platform for combating MDR bacterial infections with potential for clinical translation (Fig. 1).

2. Results and discussion

2.1. TEM analysis

Fig. 2 shows Transmission Electron Microscopy (TEM) images of the Cs/PVP nanogel formulations loaded with six different drug molecules: (a) TRZS (70–80 nm), (b) ACE (105–110 nm), (c) TRZO (35–45 nm). The technique offers a high-resolution visualization of the core morphology and size distribution of the nanogels, directly compared to the hydrodynamic sizes obtained by DLS (Fig. 4). The observed sizes are consistently smaller than those reported by DLS due to the absence of a hydrated layer in the dry state under TEM imaging. The near-spherical morphology and relatively narrow size distribution visible in the micrographs reflect uniform nanogel formation and controlled synthesis. Differences in particle size across the various formulations can be attributed to the structural and chemical nature of the encapsulated drugs, which affect the internal packing density and cross-linking behavior of the nanogel network. For instance, the larger size of the ACE-loaded nanogels (105–110 nm) suggests a more expanded matrix structure, potentially due to steric hindrance or less efficient cross-linking. In contrast, TRAZO-loaded nanogels show the smallest size (30–45 nm), indicating tighter packing or stronger drug-polymer affinity. The distinct core-shell-like contrast in some micrographs suggests phase separation within the nanogels, potentially linked to differential localization of the drug within the matrix. Overall, Fig. 3 confirms the nanoscale dimensions, structural integrity, and morphological consistency of the Cs/PVP nanogels, reinforcing their suitability for biomedical applications such as targeted drug delivery, where size and shape critically influence pharmacokinetics, cellular uptake, and biodistribution.

2.2. Nanogel UV spectrophotometric analysis

The UV spectrophotometric data in Fig. 3 illustrate the absorbance profiles of three compounds: TRZS (A), ACE (B), and TRZO (C), comparing their native form (curve 1) with their formulation in a chitosan/polyvinylpyrrolidone (Cs/PVP) nanogel (curve 2). These comparisons provide insight into how nanogel encapsulation affects the electronic environment, solubility, and potential stability of each compound. For TRZS (Fig. 3A), both curves display a prominent absorption peak within the 300–320 nm range, likely corresponding to $\pi \rightarrow \pi^*$ transitions associated with aromatic or conjugated structures. The absorbance of the native TRZS (curve 1) is higher than that of the nanogel-incorporated form (curve 2), suggesting that nanogel integration leads to reduced molar absorptivity. This reduction could be due to decreased molecular aggregation or encapsulation effects, which limit light interaction with TRZS chromophores. Additionally, a slight red shift observed in the

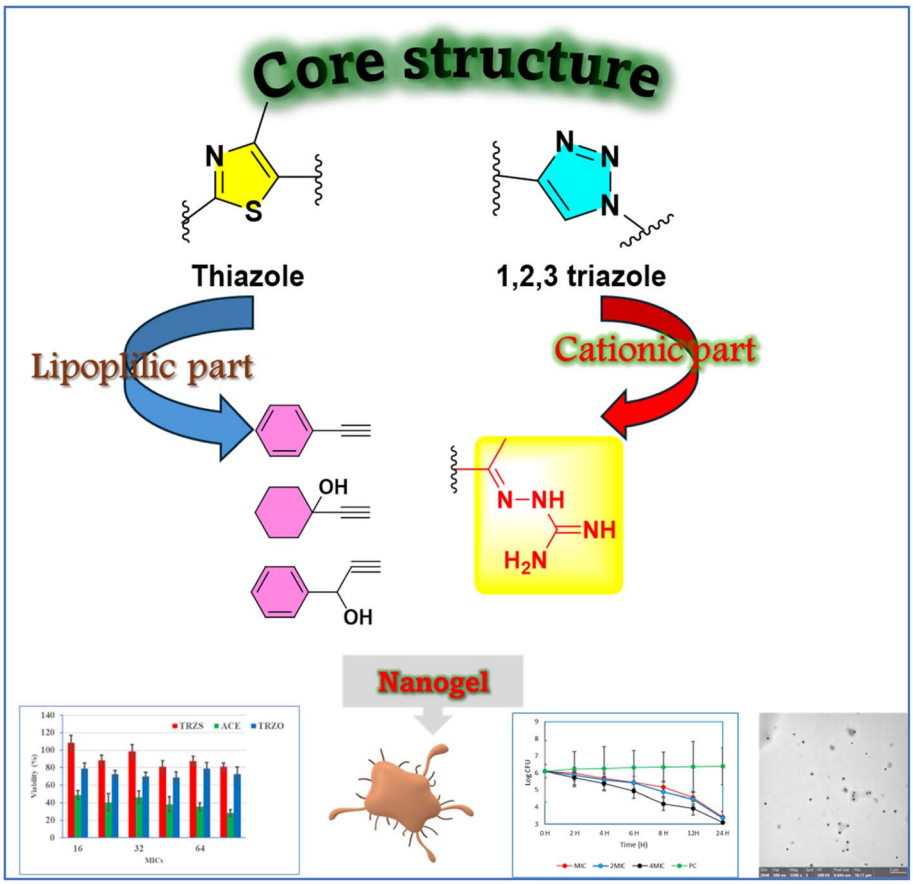

Fig. 1 Target scaffolds and nanogels with corresponding biological screens for rationalization of the study.

nanogel sample indicates possible interactions, such as hydrogen bonding, between TRZS and the Cs/PVP network. In the case of ACE (Fig. 3B), the spectra show a sharp absorption peak around 290–310 nm. Interestingly, unlike TRZS, the absorbance slightly increases in the nanogel formulation (curve 2), implying an enhancement in solubility or stabilization of ACE within the hydrophilic nanogel matrix. The unchanged peak position across both curves indicates minimal alteration of ACE's core structure but suggests beneficial interactions with the nanogel that improve its UV visibility and possibly its dispersion in aqueous media. For TRZO (Fig. 3C), the spectral range between 260–400 nm reveals that curve 1 (native TRZO) has a broader and more intense absorbance band, particularly between 280–350 nm, compared to the nanogel-incorporated form (curve 2). This attenuation in curve 2 again suggests that encapsulation in the Cs/PVP nanogel may shield the chromophores or limit their exposure to the UV beam, possibly through physical entrapment or intermolecular interactions within the polymeric network.

Overall, the UV spectroscopic profiles indicate that the incorporation of Cs/PVP nanogel has variable effects, depending on the compound. TRZS and TRZO show reduced absorbance intensity, likely due to encapsulation effects that alter chromophore accessibility or local polarity. In contrast, ACE exhibits enhanced absorbance, indicating improved solubility or molecular stabilization. These findings highlight the versatile role of Cs/PVP nanogels in modulating the optical properties of pharmaceutical compounds, supporting their potential utility in enhancing drug delivery performance through improved stability and controlled interaction with the surrounding medium.

2.3. Dynamic light scattering (DLS) analysis

Dynamic Light Scattering (DLS) analysis as shown in Fig. 4 provides significant insights into the physical properties and colloidal stability of drug-loaded Cs/PVP nanogel systems. The results demonstrate distinct variation in particle size and surface charge properties between the six drug-loaded formulations. Fig. 4 shows the dynamic light scattering analysis of drug-loaded Cs/PVP nanogel formulations for six different compounds: TRZS, ACE and TRZO. The DLS provides critical information on the hydrodynamic diameter of nanoparticles in suspension, which reflects the size of the core particle, the solvation layer, and any dynamic surface interaction. The observed sizes, 180 nm for TRZS, 277 nm for ACE, 320 nm for TRZO, demonstrate that the incorporation of each drug leads to distinct particle size distributions, influenced by drug-polymer interactions, drug solubility, molecular weight, and compatibility with the polymer matrix. The larger sizes observed for TRZO suggest stronger intermolecular interactions or possible

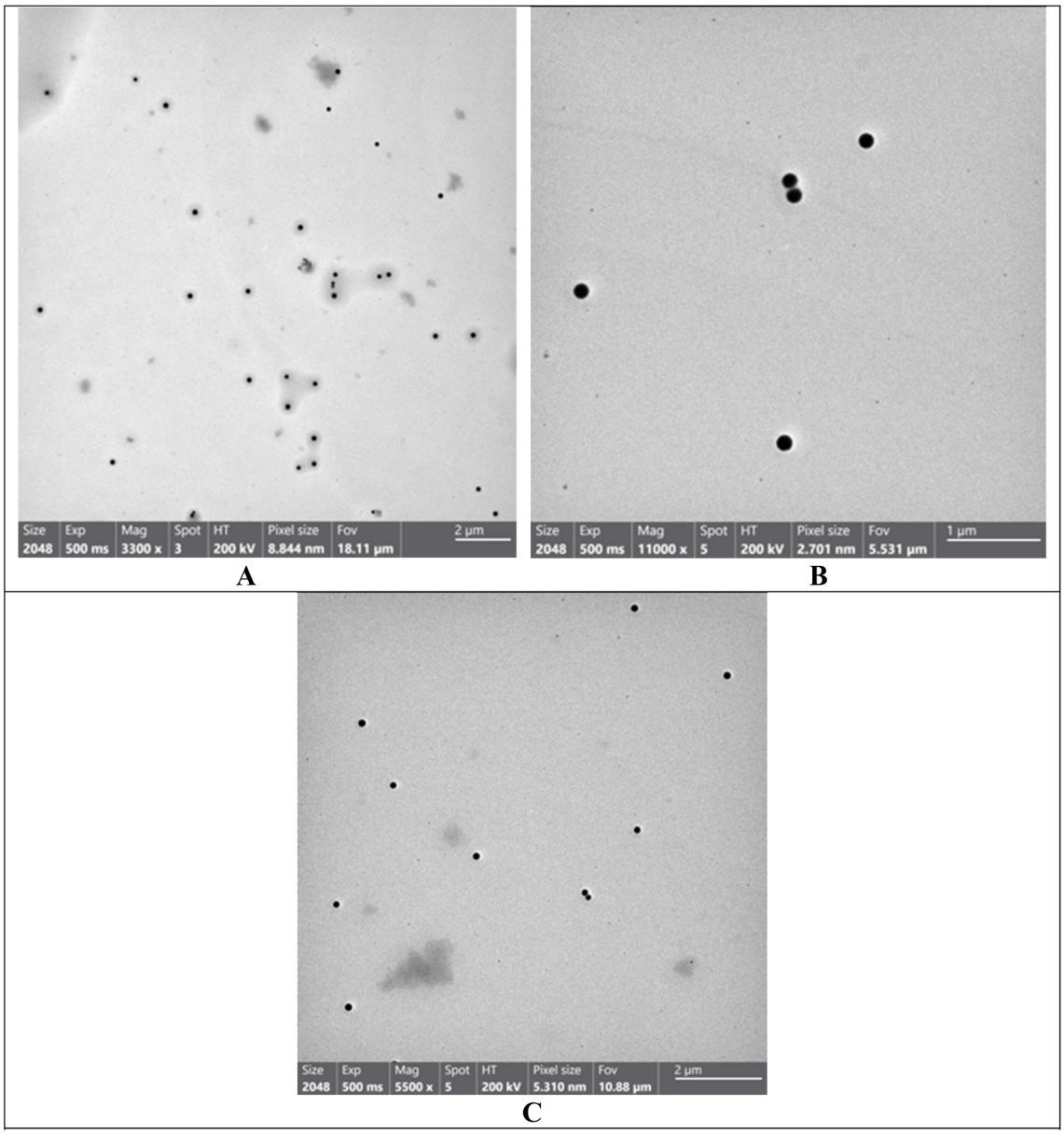

Fig. 2 TEM of (A) (Cs/PVP)TRZS nanogel with 35–45 nm (B) (Cs/PVP)ACE with 75–80 nm (C) (Cs/PVP)TRAZO with 85–90 nm.

aggregation tendencies, likely due to hydrophobicity or steric effects of the drug molecules. Conversely, TRZS relatively smaller hydrodynamic diameter indicates a more compact and stable nanogel formation with efficient encapsulation. These variations highlight the adaptive nature of the Cs/PVP nanogel system in accommodating diverse drug molecules, tailoring its size in response to the molecular characteristics of these molecules. The consistent particle sizes within the nanometric range also confirm the colloidal stability of the formulations, which is critical for biological applications such as drug delivery. Furthermore, the low polydispersity values reported elsewhere in the document support the monodispersity of these systems, highlighting the effectiveness of the synthesis and purification protocols in generating uniform and stable nanogels.

2.4. Antimicrobial efficacy of the nanogels

The antimicrobial evaluation of nanogels compared to free compounds was conducted to clarify the impact of nano-folmulation on the antimicrobial efficacy. Inhibition zone determination using the disc method was conducted for nanogels and free compounds, and data were deposited in the SI materials, Table S2 and Fig. S8. To investigate the bacterial inhibitory and killing effects of all the prepared nanogels, the minimal inhibitory concentration (MICs) of ten different Gram-positive/negative bacterial strains were determined (*E. coli* ATCC 25922, *A. baumannii* ATCC 17978, *K.pneumonia* ATCC 700603, *P. aeruginosa* ATCC 25668, *P. mirabilis* ATCC 29906, *S. aureus* ATCC 43300 MRSA, *S. spidermidis* ATCC 12228, *B. subtilis* ATCC 6633, *Micrococcus luteus* ATCC 9341, and *E. feacalis* ATCC

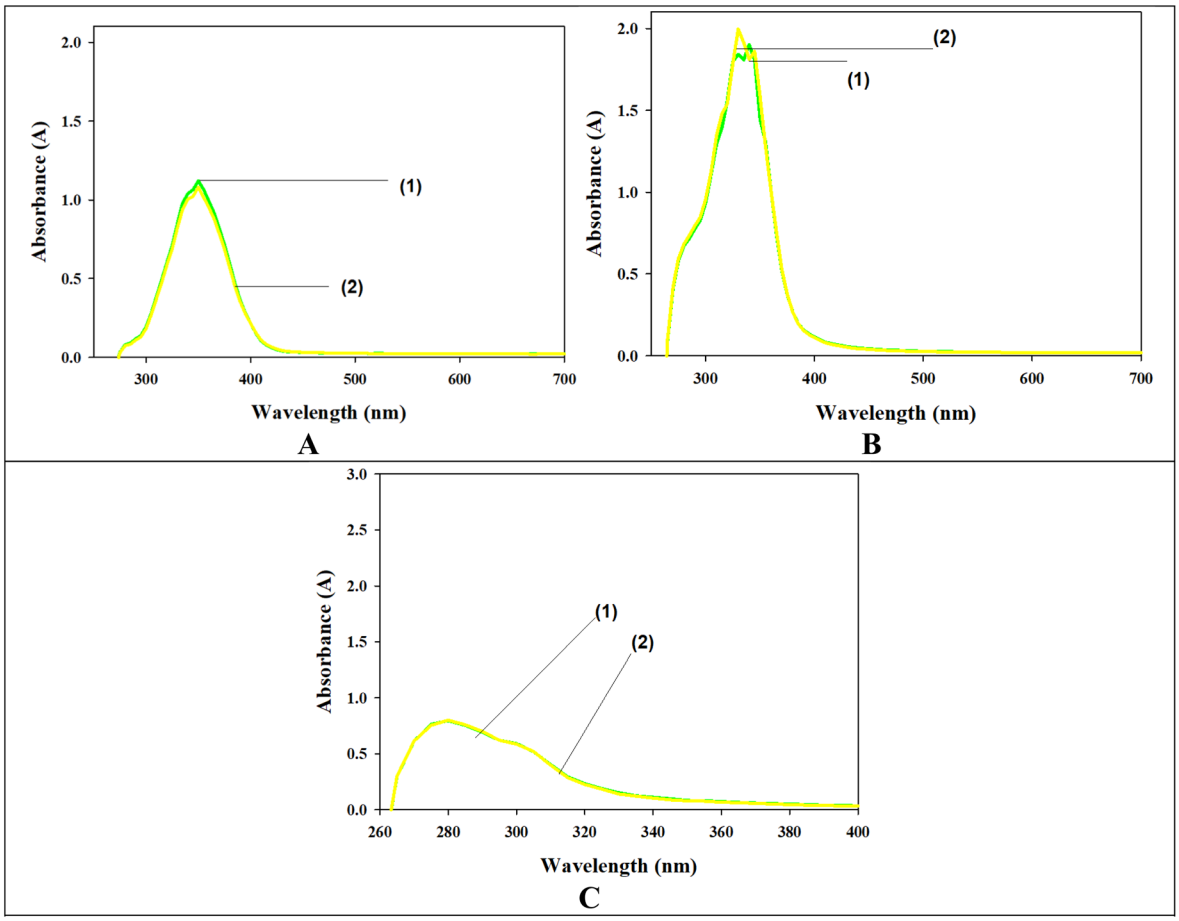

Fig. 3 UV spectrophotometer of (A) TRZS (B) ACE (C) TRZO curve 1 (sample) and 2 (sample with Cs/PVP nanogel).

29212). As shown in Table 1, the current study sought to assess and compare the antimicrobial activity of three hydrophobic compounds—phenylthiazole, phenylguanidine, and phenyltriazole—in their delivery through Cs/PVP nanogels or otherwise by their non-nanoformulated counterparts. In this respect, enhancement in antibacterial activity was assessed quantitatively through the Fold Potentiation (FP) index of their nanogels as compared to respective non-nanoformulated counterparts in terms of MIC values. Thus, it is expressed as FP = MIC(S)/MIC(Ng), where an FP value greater than one suggests that nanogels increase activity. Therefore, the lower the MIC, the stronger the agent's antibacterial activity. All three compounds had their antibacterial activity substantially improved to a great extent by the nanogel formulations against the Gram-positive strains. Among these, phenylthiazole nanogels were found, most consistently, to deliver an improved activity, especially against *S. aureus* ATCC 43300 (FP = 64), *S. epidermidis* ATCC 12228 (FP = 32), and *P. aeruginosa* ATCC 25668 (FP = 8). Such improvements were due to increased solubility and bioavailability of phenylthiazole in the ng form, which might have helped in better interaction with the bacterial membrane. Very good improvements have also been seen for nanogels of phenylguanidine, especially against *S. aureus* (FP = 32), *E. faecalis* (FP = 16), and *Bacillus subtilis* (FP = 8). This is contributed by the guanidine moiety, which facilitates electrostatic interaction with the negatively charged bacterial cell envelope, thereby leading to membrane disruption and enhanced uptake. Phenyltriazole nanogels were not quite as effective as other nanogels but gave a really positive FP value, with *S. aureus* being the best target (FP = 32) and *B. subtilis* giving (FP = 8). This shows that while the nanoformulation helps, phenyltriazole may have less inherent antimicrobial activity affected by encapsulation among the other two in the series.

The Gram-positive bacteria had a stronger response to the nanogel formulation, especially *S. aureus*, *S. epidermidis*, and *Micrococcus luteus* (FP values 8–64). It indicates a very high degree of potentiation. This may be due to the relatively simple structure of the Gram-positive bacteria's peptidoglycan-rich cell wall, which is affected more easily by such nanostructures and their cationic functional groups like guanidine. The Gram-negative, however, such as *K. pneumoniae* or *A. baumannii*, had only very limited improvements and usually had FP values ranging from 1 to 4 because of their more complex outer membrane barrier. *E. coli* and *P. aeruginosa* were exceptions regarding the Gram-negative strains. The nanogels made with phenylthiazole and phenylguanidine here achieved an FP value of 8 under optimized conditions, thereby demonstrating the ability to overcome certain permeability barriers. Moreover, the antimicrobial effect

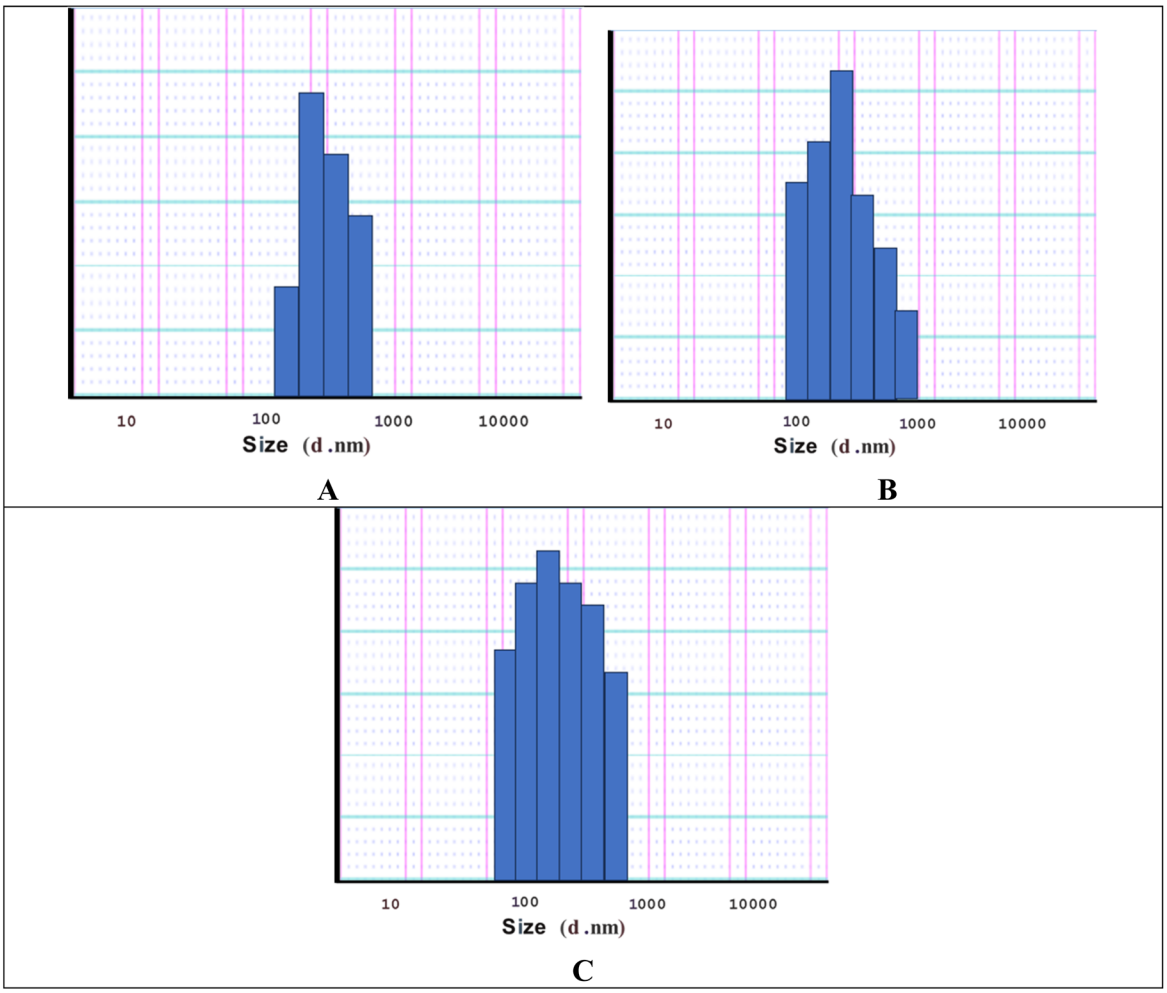

Fig. 4 DLS of (A) (Cs/PVP) TRZS nanogel (B) (Cs/PVP) ACE (C) (Cs/PVP) TRAZO.

of pure nanogel without drug loading resulted in MIC values exceeding 512 μg mL^{-1}, confirming the compounds' potency. Overall, these results substantiate yet another very novel application of nanogels for carrying hydrophobic agents, the antimicrobial nature of which is to be enhanced.[34,36,43,44] The Cs/PVP nanogel would also possess solubility and retention properties, along with dual-action mechanisms that target both UPP synthetase and DNA gyrase, thus hampering bacterial cell-wall

Table 1 Antibacterial data of nanogels (Ng) and free sample (S) of target compounds against different strains as MICs values in μg mL^{-1}

	MICs values in μg mL^{-1}[a]								
	TRZS			ACE			TRZO		
Strains	Ng	S	FP	Ng	S	FP	Ng	S	FP[b]
E. coli ATCC 25922	32	256	8	64	512	8	128	256	2
A. baumannii ATCC 17978	128	1024	8	64	256	4	512	512	1
K.pneumonia ATCC 700603	1024	1024	1	256	1024	4	1024	1024	1
P. aeruginosa ATCC 25668	64	512	8	128	1024	8	256	1024	4
P. mirabilis ATCC 29906	512	512	1	256	1024	4	256	512	2
S. aureus ATCC 43300 MRSA	8	512	64	4	128	32	4	128	32
S. spidermidis ATCC 12228	32	1024	32	32	64	2	64	128	2
B. subtilis ATCC 6633	64	128	2	32	256	8	128	1024	8
Micrococcus luteus ATCC 9341	128	256	2	64	128	2	128	1024	8
E.feacalis ATCC 29212	512	512	1	64	1024	16	512	1024	2

[a] MIC values were obtained from a singlet experiment. [b] FP = MIC (S)/MIC (Ng).

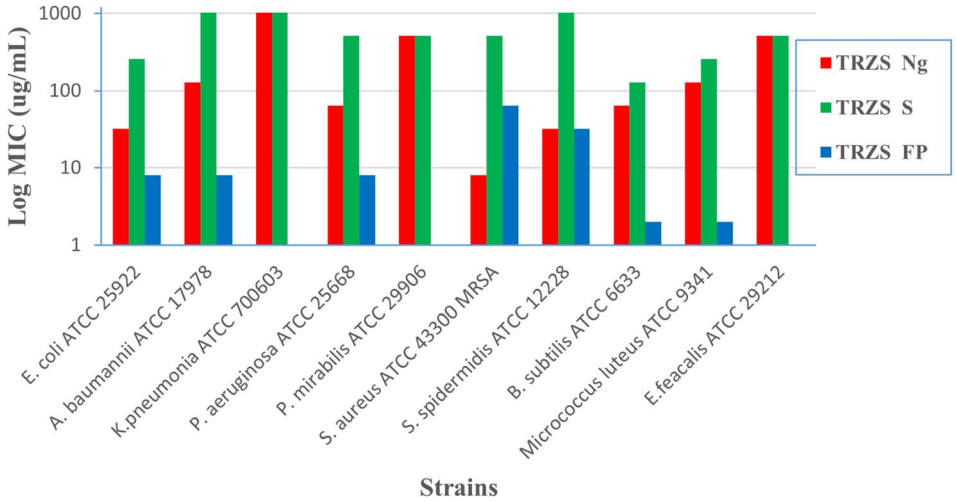

Fig. 5 MIC folds reduction and of TRZS free compound (S) and loaded-nanogel (Ng) against different bacterial strains.

synthesis and stopping DNA replication. Guanidine moieties in the structure further enhance this property, providing a means for targeted electrostatic interactions with the bacterial membrane. In general, the delivery through nanogels results in a substantial increase in the antibacterial activity of all the compounds considered, with higher effects noted for those systems based on phenylthiazole against resistant Gram-positive strains. The data further justified the need to design and develop Cs/PVP nanogels to combat MDR infections, especially those caused by Gram-positive pathogens (Fig. 5–7).

2.5. Mechanism of hydronanogels antibacterial action

Hydronanogels were successfully formed by mixing polyvinylpyrrolidone (PVP) and chitosan with various small-molecule chemical scaffolds, including phenyltriazole, phenylthiazole, and aryl carboximidamides. When incorporated into the polymeric matrix, these scaffolds produced nanostructured hydrogels with enhanced antibacterial activity compared to the individual compounds. The observed potentiation is hypothesized to arise from the formation of physical complexes driven by multiple non-covalent interactions such as hydrogen bonding and electrostatic interactions. Chitosan, with its protonated amino groups, offers strong electrostatic attraction to negatively charged bacterial membranes, while also forming hydrogen bonds with functional groups on the small molecules. PVP, possessing a lactam carbonyl group, further stabilizes the system *via* hydrogen bonding with amines, imidamides, and heterocycles present in the scaffolds. These synergistic interactions not only improve drug dispersion and

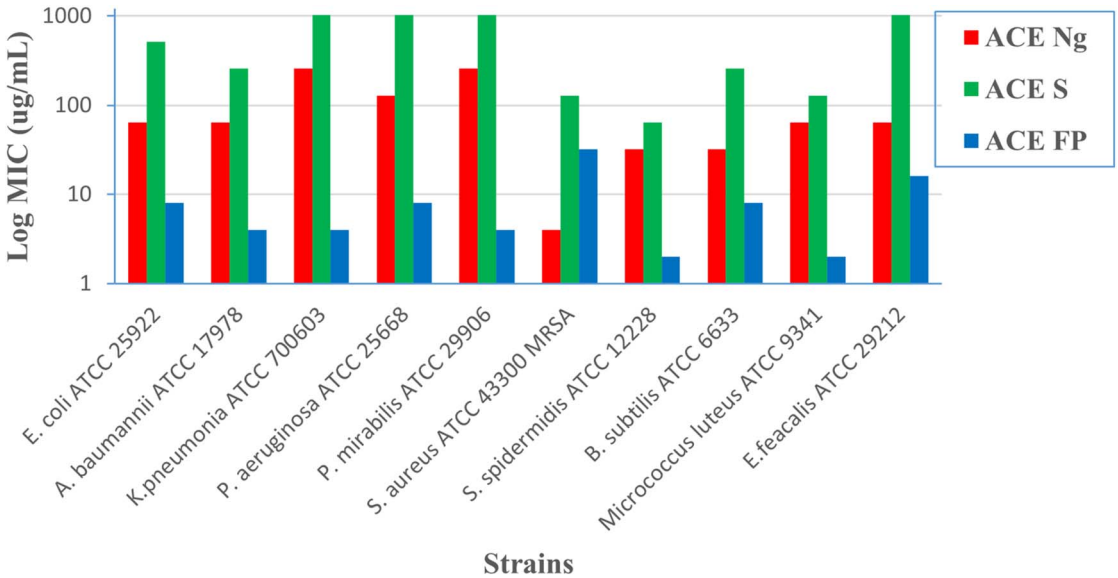

Fig. 6 MIC folds reduction and of free ACE compound (S) and loaded-nanogel (Ng) against different bacterial strains.

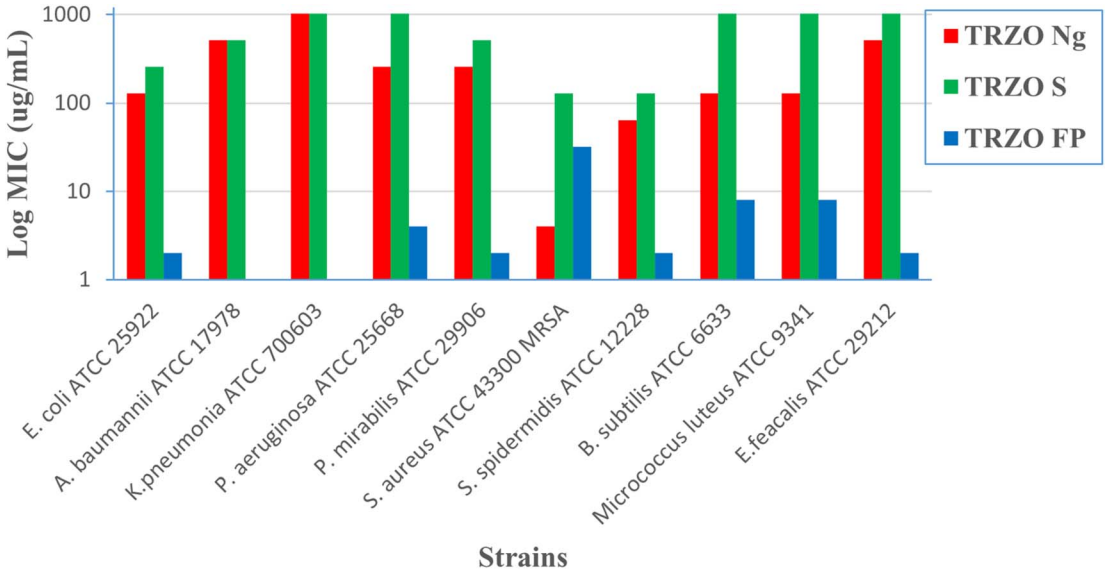

Fig. 7 MIC fold reduction and of free TRZO compound (S) and loaded-nanogel (Ng) against different bacterial strains.

retention but also enhance bacterial membrane disruption, leading to superior antibacterial performance (Fig. 8).

The differential antibacterial responses observed between Gram-positive and Gram-negative bacteria can be explained by their distinct cell wall architectures. Gram-positive bacteria possess a thick peptidoglycan layer that, despite its density, is relatively porous and permits easier penetration of nanogels. In addition, electrostatic interactions between the cationic nanogels and the negatively charged cell wall components further facilitate membrane disruption and drug delivery. By contrast, Gram-negative bacteria contain an additional lipopolysaccharide-rich outer membrane, which acts as a permeability barrier and limits nanogel uptake, thereby reducing their responsiveness. Interestingly, exceptions such as *Escherichia coli* and *Pseudomonas aeruginosa* demonstrated improved susceptibility when treated with nanogels, which may be attributed to enhanced permeability and partial overcoming of efflux mechanisms mediated by the nanogel system.

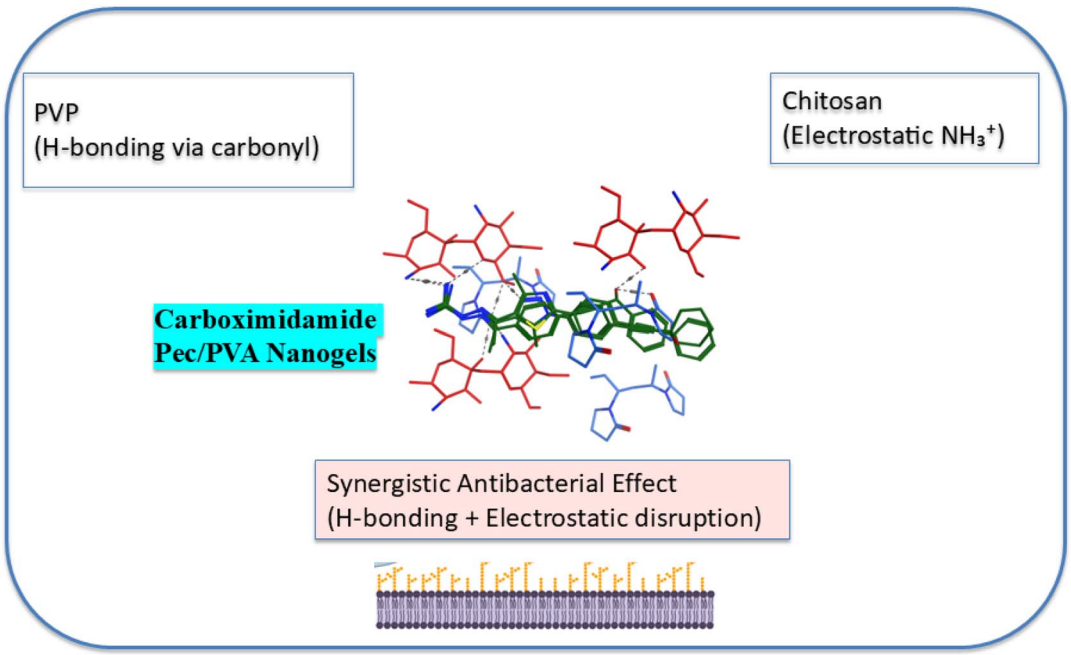

Fig. 8 A schematic-style figure illustrating the formation of antibacterial hydronanogels through the interaction of PVP, chitosan, and various small-molecule scaffolds. It shows the key interactions (hydrogen bonding and electrostatic attraction) and highlights the enhanced antibacterial activity.

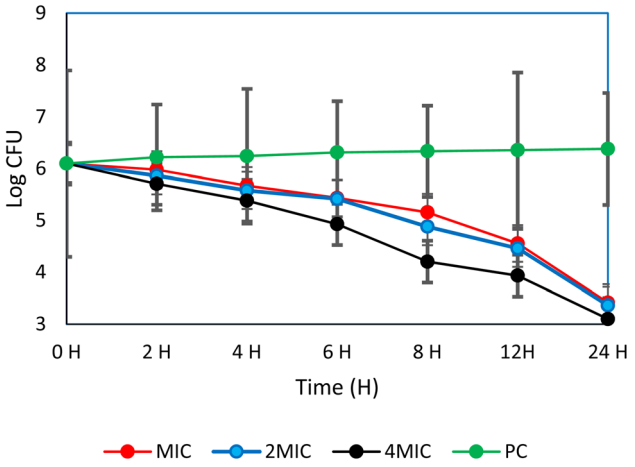

Fig. 9 Time-killing analysis of TRZS-ng against MRSA over a 24-hour incubation period at 37 °C. SE are presented on the chart.

2.6. Time-killing assay against MRSA strain

Methicillin-resistant *Staphylococcus aureus* (MRSA) remains among the most challenging bacterial pathogens. It is responsible for several difficult-to-treat infections due to its resistance to commonly used antibiotics, including methicillin and other β-lactams. This growing resistance has led to an urgent need for new antimicrobial agents to effectively combat MRSA infections. In this context, vancomycin, a glycopeptide antibiotic, has been a mainstay in the treatment of MRSA; However, increasing resistance and sometimes limited effectiveness have driven the search for alternative therapies. To address this issue, the most potent hydronanogel formulation of TRZS with more FP value, 64, was evaluated for its antibacterial activity (Fig. 5) against methicillin-resistant *Staphylococcus aureus* (MRSA) over 24 hours. The *y*-axis represents the logarithm of colony-forming units per milliliter (CFU mL^{-1}) of MRSA and indicates bacterial concentration, while the *x*-axis shows time in hours (Fig. 9).

The figure presents the results of a time-kill assay for compound TRZS nanogel against MRSA, showing the reduction in bacterial load over time at different concentrations relative to the minimum inhibitory concentration (MIC). The concentrations tested include MIC, 2MIC, 4MIC, and a positive control (PC). The graph indicates that higher concentrations of TRZS nanogel lead to a more rapid and significant reduction in bacterial counts, with the 4MIC and PC showing the most pronounced effects. These results are significant as they demonstrate the dose-dependent bactericidal activity of TRZS gel against *B. subtilis*. The compound's effectiveness at concentrations above the MIC suggests its potential as an antimicrobial agent, particularly in the context of treating infections caused by MRSA. Further research and development could lead to new treatment options for infections where conventional antibiotics may be ineffective due to resistance or other factors (Table 2, and Fig. 9).

2.7. Inhibitory DNA gyrase supercoiling assay

Nanogels have emerged as efficient nanocarriers for antimicrobial delivery due to their ability to enhance drug solubility, protect labile compounds, and facilitate targeted delivery to bacterial enzymes and intracellular sites, thereby significantly improving antibacterial activity.[45,46] The comparative evaluation of Cs/PVP nanogels loaded with phenyltriazole (TRZS), phenylthiazole (ACE), and phenylguanidine (TRZO) compounds *versus* their free forms demonstrated that nanogel encapsulation significantly enhanced antimicrobial potency. This enhancement is quantitatively supported by the Fold Potentiation (FP) indices observed across key bacterial targets, namely DNA gyrase. Notably, among the tested compounds, TRZS-Ng exhibited the highest inhibitory potency against DNA gyrase ($IC_{50} = 4.44 \pm 0.18$ μg mL^{-1}), showing a 5.77-fold improvement over free TRZS (25.6 ± 1.54 μg mL^{-1}). TRZO-Ng and ACE-Ng also showed enhanced activity with IC_{50} values of 14.13 ± 0.57 μg mL^{-1} and 21.09 ± 0.85 μg mL^{-1}, corresponding to 2.09- and 1.56-fold increases in potency compared to their free forms, respectively. These enhancements can be attributed to the nanogels' ability to improve drug solubility and stability, facilitate sustained release, and potentially enhance interaction with the bacterial enzyme active site.

When compared to the reference drug novobiocin ($IC_{50} = 0.55 \pm 0.022$ μg mL^{-1}), a well-established DNA gyrase inhibitor, TRZS-Ng demonstrated a relatively high level of inhibition, suggesting its potential as an effective alternative when

Table 2 Time-killing analysis including log CFU values of bacterial cells at different incubation periods (0–24 h) in the presence of TRZS nanogel at concentrations corresponding to 1MIC, 2MIC, and 4MIC compared with positive control (PC). Data are expressed as mean ± SE ($n = 3$)

Incubation period (hrs)	Concentration (μg mL^{-1})			
	1MIC	2 MIC	4 MIC	PC
	Log CFU			
0 H	6.097 ± 0.1	6.097 ± 0.88	6.097 ± 1.1	6.097 ± 1.8
2 H	5.978 ± 0.58	5.863 ± 1.1	5.708 ± 1.3	6.217 ± 1.02
4 H	5.672 ± 0.68	5.58 ± 1.5	5.384 ± 1.0	6.241 ± 1.3
6 H	5.436 ± 1.2	5.417 ± 1.1	4.929 ± 0.77	6.312 ± 0.99
8 H	5.158 ± 1.3	4.881 ± 0.58	4.204 ± 0.98	6.334 ± 0.89
12 H	4.556 ± 0.91	4.461 ± 0.98	3.934 ± 1.01	6.356 ± 1.5
24 H	3.417 ± 1.0	3.362 ± 1.41	3.1 ± 0.99	6.38 ± 1.08

Table 3 The inhibitory enzyme assay data of free compounds and nanogels (IC_{50} (μg mL^{-1})[a]

Cp.		DNA gyrase
TRZS	Ng	4.44 ± 0.18
	S	25.6 ± 1.54
	FP	5.77
ACE	Ng	21.09 ± 0.85
	S	32.8 ± 2.91
	FP	1.56
TRZO	Ng	14.13 ± 0.57
	S	29.5 ± 4.10
	FP	2.09
Novobiocin		0.55 ± 0.022

[a] Ng; nanogel formulations, S; free compounds, FP; fold potency. IC_{50} ± SE values (μg mL^{-1}) for at least three runs; compound concentration required to produce 50% inhibition of supercoiling of DNA gyrase enzyme. Data are presented as average IC_{50} ± SD.

delivered *via* nanogel formulation. Although not surpassing novobiocin in absolute potency, the nanogel-loaded TRZS represents a promising candidate due to its dual-target capability and improved delivery characteristics.

Overall, these results highlight the beneficial role of nanogel encapsulation in enhancing the inhibitory effect of antibacterial compounds on DNA gyrase, supporting its utility as a strategy to improve the efficacy of existing or novel antimicrobial agents,[23] Table 3.

2.8. Anti-biofilm effect

2.8.1. Biofilm inhibition efficacy. A crucial factor in the development of new antibiotics is their ability to inhibit bacterial virulence mechanisms, particularly biofilm formation. This study evaluated the anti-biofilm potential of three compounds: TRZS, TRZO, and ACE, administered both as free agents and nanogel encapsulated (NGs) against two clinically important biofilm-producing pathogens, *Pseudomonas aeruginosa* and methicillin-resistant *Staphylococcus aureus* (Table 4, and Fig. 10). Nanogel encapsulation effectively enhanced biofilm inhibition in all the formulations under test, making the use of nanogel-based delivery systems suitable for treating resistant biofilm-related infections. Against *P. aeruginosa*, NG formulations in all cases were superior in performance compared to their free compound analogues. TRZS nanogels were inhibited by 53% *versus* 44% by free TRZS, and TRZO NGs showed a significant improvement from 35% (free) to 69% (NG). Similarly, ACE NGs modestly improved inhibition from 34% to 40%. The enhanced potency of TRZO NGs *versus P. aeruginosa* was of particular importance, suggesting that this compound can benefit most from nanogel encapsulation, perhaps due to better penetration within the biofilm matrix or local retention. In contrast to MRSA, the benefit of NG encapsulation was more pronounced. TRZS NGs yielded an impressive 79% inhibition compared to merely 29% for the free drug a greater than 2.5-fold enhancement. TRZO was also more active encapsulated (55% *vs.* 28%), and ACE NGs improved biofilm inhibition from 28% to 41%. These results indicate the ability of NGs to greatly increase the efficacy of otherwise relatively weakly active compounds against MRSA biofilms, which are notoriously refractory to treatment due to their dense extracellular matrix and resistance mechanisms. Several factors likely explain the improved performance of NG formulations. Nanogels provide a protective environment to the active agent, with increased solubility and stability. Their nanometer size and hydrophilicity can also promote penetration into the dense biofilm matrix, and controlled release from the NGs maintains effective local drug concentrations for extended periods. The NG matrix may also exhibit stronger interactions with the negatively charged bacterial surface or the EPS, promoting more efficient disruption of the biofilm. These findings corroborate earlier research highlighting the role of nanocarriers in bypassing biofilm-induced resistance. However, the current research presents a comparative evaluation of compound classes and pathogens, showing a broader perspective towards nanogel potential as global biofilm inhibitors. In general, nanogel encapsulation significantly amplified the biofilm inhibition activity of TRZS, TRZO, and ACE, particularly towards MRSA. These observations attest to the utility of NG-based delivery systems for enhancing the therapeutic efficacy of anti-biofilm drugs and warrant further evaluation in preclinical infection models in terms of safety, pharmacokinetics, and *in vivo* characteristics.

Table 4 Percentage of biofilm inhibition (mean ± SE, $n = 3$) of TRZS, TRZO, ACE, and their corresponding nanogel formulations (TRZS ng, TRZO ng, ACE ng) against *P. aeruginosa* and MRSA strains

Cp.	Biofilm inhibition %	
	P. aeruginosa	MRSA
TRZS	44 ± 3.50	29 ± 2.10
TRZS ng	53 ± 3.10	79 ± 2.91
TRZO	35 ± 4.50	28 ± 3.01
TRZO ng	69 ± 4.70	55 ± 4.81
ACE	34 ± 2.01	28 ± 2.20
ACE ng	40 ± 5.21	41 ± 2.70

2.8.2. Biofilm clearance efficacy. Biofilms are complex, structured communities of bacteria encased in a self-produced extracellular matrix, representing a crucial virulence factor for both *Pseudomonas aeruginosa* and *Staphylococcus aureus*. These biofilms confer significant resistance to conventional antibiotics and host immune defenses, often leading to persistent and recalcitrant infections. The present study tested the biofilm-disrupting ability of the three antimicrobial compounds TRZS, TRZO, and ACE alone or in nanogel (NG) form against established mature biofilms by *Pseudomonas aeruginosa* and methicillin-resistant *Staphylococcus aureus* (MRSA). The testing of TRZS, TRZO, and ACE compounds, both as free compounds and nanogel (NG) formulations, for the evaluation of their ability to break biofilms, indicated that encapsulation in nanogels was likely to enhance the biofilm-breaking activity in two clinically important pathogens: *Pseudomonas aeruginosa* and MRSA (Table 5 and Fig. 11). Although performance varied between compounds, the nanogel formulations in all cases enhanced or maintained the activity compared to their free

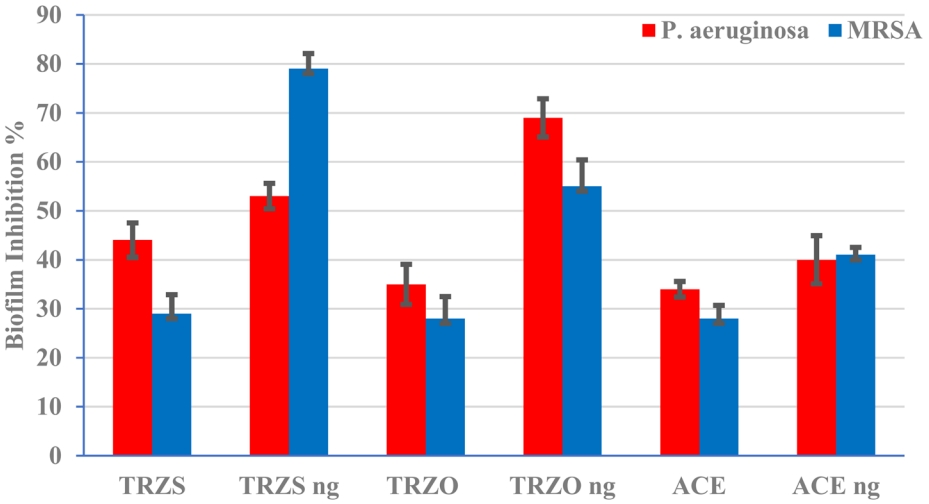

Fig. 10 Biofilm clearance efficacy of the nanogel formulations compared to free compounds against the biofilm of *P. aeruginosa* and MRSA strains. Data are represented as triplicate mean ± SE.

Table 5 Percentage of biofilm breaking/eradication activity (mean ± SE, $n = 3$) of TRZS, TRZO, ACE, and their nanogel formulations against *P. aeruginosa* and MRSA strains

Cp.	Biofilm breaking %	
	P. aeruginosa	MRSA
TRZS	5 ± 0.5	28 ± 3.9
TRZS ng	29 ± 2.6	33 ± 4.1
TRZO	13 ± 2.1	32 ± 3.8
TRZO ng	12 ± 1.9	44 ± 5.1
ACE	40 ± 5.1	10 ± 1.8
ACE ng	55 ± 5.8	27 ± 2.9

counterparts, suggesting the potential of nanogels for the treatment of mature biofilms. Among the free compounds, ACE showed the highest activity against *P. aeruginosa* (40%), while TRZO and TRZS showed moderate activities (13% and 5%, respectively). Conversely, against MRSA, TRZO (32%) and TRZS (28%) showed higher activity than ACE (10%). This control variation indicates the inherent difference in how each compound works against the biofilm matrices of different pathogens. Nanogel encapsulation significantly enhanced the biofilm-breaking activity in most cases. For instance, TRZS increased from 5% (free) to 29% (NG) in *P. aeruginosa* and from 28% to 33% in MRSA, with increased activity in both strains. TRZO NGs, while not more active in *P. aeruginosa* (12% *vs.* 13%), did show a large increase in MRSA (44% *vs.* 32%), the highest biofilm disruption observed in this study.[47] ACE, whose effectiveness was variable when in its naked state, was significantly enhanced through nanogel delivery, rising to 55% against *P. aeruginosa* and to 27% against MRSA, demonstrating nanogels' capability of enhancing subpar agents, These results show that nanogels can improve

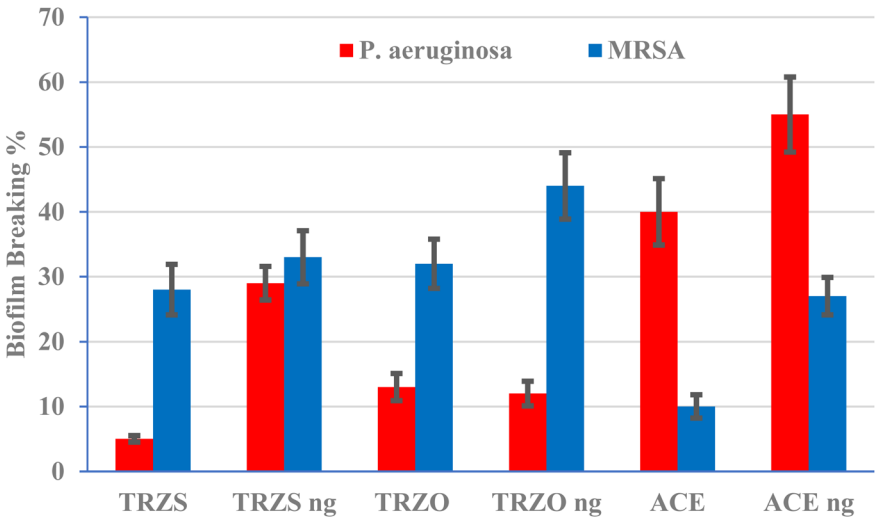

Fig. 11 Biofilm inhibition efficacy of the nanogel formulations compared to free compounds against the biofilm of *P. aeruginosa* and MRSA strains. Data are represented as triplicate mean ± SE.

Table 6 Cell viability percentages (mean ± SE, $n = 3$) of tested compounds (TRZS, TRZO, ACE) at different MICs concentrations (16, 32, and 64 μg mL^{-1}) in a human diploid fibroblast cell line (WI-38)

Cp.	Viability assay (%) using MICs values in (μg mL^{-1})					
	16		32		64	
TRZS	108.5 ± 8.5	88.5 ± 5.8	98.6 ± 7.5	80.9 ± 6.9	87.5 ± 5.3	80.9 ± 4.5
ACE	48.6 ± 4.9	40.5 ± 9.5	46.5 ± 6.8	38.4 ± 8.5	35.5 ± 4.6	28.5 ± 3.9
TRZO	78.9 ± 6.5	72.6 ± 4.3	69.8 ± 4.9	68.5 ± 6.4	78.9 ± 6.9	72.6 ± 7.9

drug delivery by a variety of mechanisms: by protecting active agents from degradation, enhancing penetration into the dense biofilm matrix, and controlled release to maintain local therapeutic concentrations. Improvements were especially critical for drugs that are initially weak or of intermediate activity, such as TRZS and ACE, which suggests that nanogels could rescue or enhance the clinical usefulness of current antimicrobials. The strain-dependent variations also suggest that the interaction between the nanogel, the compound, and the specific biofilm microenvironment is critical to the outcome.

2.9. Cellular biocompatibility of nanogels

Any antimicrobial agent or nanocarrier intended for therapeutic use must be biocompatible. An ideal antimicrobial system would be one that is highly active against pathogenic bacteria but has minimal toxicity to the host tissue cells. In order to check the safety of the synthesized Cs/PVP nanogels, *in vitro* cytotoxicity was evaluated in a human diploid fibroblast cell line (WI-38), which is the standard model for preliminary biocompatibility screening.

The cytotoxicity assay was performed at a range of nanogel concentrations (16, 32, and 64 μg mL^{-1}), and the cell viability (%) using MTT methodology for each formulation is summarized in Table 6 and Fig. 12. The results showed that the formulations nanogel are significantly more biocompatible than their non-nanoformulated counterparts.

Among the tested nanogels, the phenylthiazole carboximidamide nanogel demonstrated the highest degree of biocompatibility, maintaining over 88% cell viability at 32 μg mL^{-1} and 80.9% even at 64 μg mL^{-1}. This suggests that the nanocarrier system effectively modulates the cytotoxic effects of the active compound, potentially through controlled release and reduced nonspecific interactions with host cells.

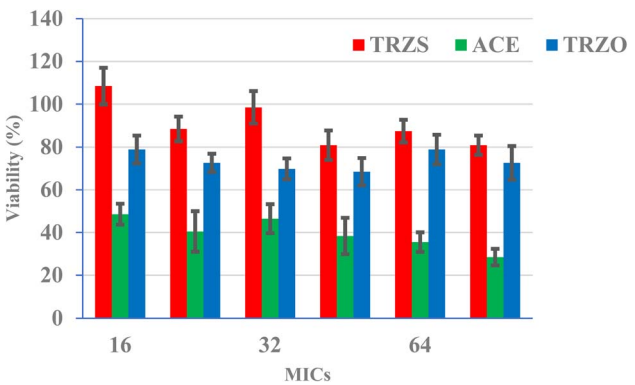

Fig. 12 The effect of nanogels on human diploid fibroblast cell line (WI-38) cell viability was extended for 48 h at 37 °C, respectively. The cytotoxicity was determined by MTT assay. Data are represented as triplicate mean ± SE.

In contrast, the free phenyl carboximidamide (non-nanoformulated) exhibited the highest cytotoxicity, with cell viability dropping below 40% at 32 μg mL^{-1} and further declining to 28.5% at 64 μg mL^{-1}, indicating substantial toxicity at therapeutically relevant concentrations. This stark contrast highlights the protective and biocompatible nature of the Cs/PVP nanogel matrix, which likely minimizes direct exposure of fibroblasts to the free drug.

The phenyltriazole carboximidamide nanogel also demonstrated acceptable biocompatibility, with cell viabilities ranging from 69.8% to 78.9% across tested concentrations, reflecting a favorable safety profile.[48] The impurity profiles of the synthetic route of the nanogels preparation were toxicologically characterized using MTT assay (Cs/PVP system) against the WI-38 cell line, with viability data 89% and cytotoxicity of 11% which reverses the safety profile of the containing materials. The antibacterial effects observed here are consistent with earlier studies reporting phenylthiazoles as potent enzyme inhibitors,[21] triazoles as scaffolds enhancing antimicrobial binding and solubility,[42,49] and guanidine groups as strong cationic motifs that disrupt bacterial membranes.[27,50] Compared with these reports, our Cs/PVP nanogel formulations achieved greater MIC fold potentiation and superior biofilm inhibition, highlighting the synergistic advantage of nanogel encapsulation in amplifying the intrinsic activities of these pharmacophores.

Collectively, these findings demonstrate that nanogel encapsulation significantly enhances the biocompatibility of the tested antimicrobial agents. The Cs/PVP nanogel system appears to provide a safe and efficient platform for delivering hydrophobic antibacterial agents, reducing off-target toxicity while maintaining potent antibacterial effects. This balance between efficacy and safety underscores the potential of these nanogels as viable candidates for further *in vivo* evaluation and clinical development.

2.10. Correlative nanocharacterization and structure–activity relationships

The physicochemical characterization of the nanogels was evaluated by correlating TEM, DLS, and UV-Vis analyses and linking these findings to the chemical structures of TRZS, TRZO, and ACE and their corresponding antimicrobial profiles. TEM

imaging confirmed that all nanogels possessed well-defined spherical morphology in the dry state, with diameters in the 35–110 nm range. DLS measurements demonstrated larger hydrodynamic sizes (180–320 nm) due to solvation shells and hydration layers, with narrow distributions and stable zeta potentials, confirming excellent colloidal stability. UV-Vis spectra showed reduced aggregation signatures and improved solubility for all encapsulated scaffolds compared to their free counterparts, indicating that nanogel encapsulation suppressed π–π stacking and aggregation in aqueous environments.

Structural features strongly influenced nanoscale control and biological performance. TRZS, which contains a thiazole ring and a guanidinium moiety, displayed compact TEM morphology, narrow DLS distributions, and marked suppression of aggregation peaks in UV-Vis. These features translated into the highest antibacterial potentiation, with a DNA gyrase inhibition IC_{50} of 4.44 μg mL^{-1} and MRSA biofilm inhibition up to ~79%. TRZO, bearing a triazole ring, guanidinium tail, and phenolic OH group, exhibited slightly larger hydrated sizes due to increased interfacial hydration but maintained excellent colloidal stability. Its UV-Vis spectra confirmed stable dispersion, correlating with superior antibiofilm performance against Gram-negative bacteria such as *P. aeruginosa* (biofilm inhibition ~69%). ACE, incorporating a phenylthiazole scaffold with a terminal hydrophilic substituent, demonstrated highly stable DLS profiles and minimal spectral drift in UV-Vis, reflecting enhanced dispersion and solubilization. While its antibacterial potentiation was moderate relative to TRZS, ACE-nanogels showed consistent stability and effective bioactivity, suggesting a mechanism more reliant on membrane interaction and uptake than direct enzyme inhibition.

Taken together, the congruence of TEM, DLS, and UV-Vis data confirms nanoscale gel-state control across all three formulations, while differences in chemical motifs explain the distinct antimicrobial performance. TRZS-nanogels benefited most from strong electrostatic and π-interactions, TRZO-nanogels leveraged hydration and sustained release for Gram-negative activity, and ACE-nanogels offered superior stability with reliable though comparatively lower potentiation. These correlations emphasize that nanoscale architecture and scaffold chemistry jointly determine the enhanced antimicrobial profiles observed.

2.11. Pharmacophoric molecular analyses

The pharmacophore analysis of the analogs ACE, TRZO and TRZS reveals their crucial similarities and differences in the spatial orientation and functional group nature of the binding activity. Three compounds have been mapped to a generic pharmacophore model with six feature: aromatic (Aro), hydrophobic/aromatic (Hydr/Aro), hydrogen bond donor (Don), dual donor/acceptor (Don/Acc), donor (Don), and acceptor (Acc) groups. This model, based on feature, defines the key interactions required for effective binding to the target enzyme. The alignment of the molecules exhibited good overlap of the pharmacophoric features, indicating that despite structural diversity, the ligands could bind in analogous binding cavities. Measurement of distances between the pharmacophoric features gives further insight into their 3D distribution. The Aro–Hydr/Aro distance of 7.70 Å defines the spatial extent of the lipophilic/aromatic region, a pharmacophore region of primary importance for fitting into hydrophobic pockets. The Aro–Acc distance of 3.56 Å and Acc–Don distance of 2.82 Å define the proximity of the points of polar interaction, suggesting that hydrogen bonding and dipole interactions are favorably oriented in all compounds. Besides, the Acc–Don/Acc distance of 3.58 Å supports the multifunctional hydrogen bonding ability in similar positions. The aromatic nuclei of the two compounds are significant contributors to pharmacophoric alignment and interaction potential. ACE contains a benzene ring, with classical aromaticity and planarity, which enables π-stacking potential. TRZS contains a thiazole ring, which has the combination of aromaticity and the potential to act as a weak hydrogen bond acceptor *via* its heteroatoms. TRZO, which contains the triazole ring, has an intense electron density and potential for both aromatic interaction and metal coordination or polar contacts, making it highly versatile.

Finally, despite differences in their core aromatic scaffolds, all three compounds exhibit well-aligned pharmacophore features, which suggests that they share a common mode of interaction concerning the biological target. Differences in aromatic groups can adjust binding specificity and affinity, with TRZO and TRZS potentially offering more interaction versatility through their heterocyclic systems. This pharmacophore model confirms the observation that these compounds are worthy of being used as leads for optimization as enzyme inhibitors, with TRZO and TRZS delivering slightly more pharmacophoric complexity and potential (Table 7).

2.12. Molecular docking analyses

Docking analysis of the compounds ACE and TRZS compared to the bound ligand of the DNA gyrase enzyme, revealed that both compounds interact effectively with key residues in the active site of DNA gyrase B through specific fragments responsible for hydrogen bonding, hydrophobic, and aromatic interactions. ACE demonstrates the closest similarity to the reference ligand in forming hydrogen bonds *via* its N–H and C=N fragments with water molecules HOH572/HOH407 and Arg76, as well as through an OH group with Asp73—all interactions also observed in the reference, which uses its COOH and NH groups to bind Arg76, Arg136, and Asp73. ACE also establishes hydrophobic contacts through its CH_3 group with Pro79 and utilizes two phenyl rings: one forming hydrophobic interaction with Asn46, and the other participating in aromatic stacking with Val120, Ile94, and Ala47, akin to the $DiCl_2$ group in the reference. In contrast, TRZS, while not interacting with Arg76 or Arg136, maintains hydrogen bonding *via* its N–H and OH groups with HOH572/HOH407 and Asp73, respectively. It also engages in hydrophobic interaction *via* a CH_3 group with Pro79, and utilizes a triazole ring for aromatic interaction with Asn46, and a cyclohexyl ring for hydrophobic interaction with Val120, Ile94, and Ala47.

Overall, ACE has the most comparable interaction profile to the reference ligand, and efficiently reproduces both polar and non-

Table 7 Molecular analysis of target compounds, including alignment and pharmacophoric points matching

Compounds	ACE	TRZS	TRZO
Pharmacophore model	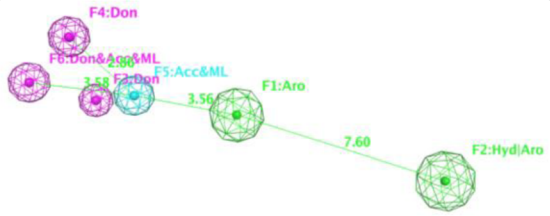		
Molecular alignment	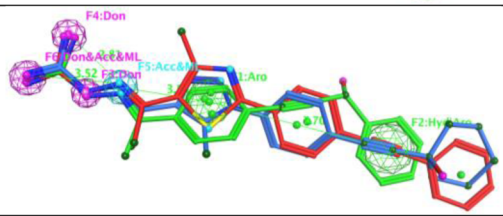		
Featuers	Aro, Hydr/Aro, Don, Don/Acc, Don, Acc		
Distances (Å)	Aro-----Hyd/Aro (7.70) Aro----------Acc (3.56) Acc----------Don (2.82) Acc----------Don/Acc (3.58)		
Aromatic part	Benzene	Thiazole	Triazole
	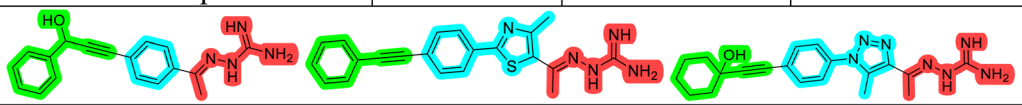		

polar interactions. In addition, TRZS introduces a new scaffold with promising binding characteristics that may further optimise the inhibition of DNA gyrase B (Table 8). Although these compounds are effective in the UPPS target, results for ACE and TRZS in the Undecaprenyl Diphosphate Synthase (UPPS) indicate that both compounds interact with key residues in the active site, although TRZS has a stronger binding profile. The ACE forms multiple hydrogen bonds with residues such as Phe70, Ser72, Ala47 and water molecule, and establishes a π–H interaction with Ala69, but with moderate binding energies (around −0.5 to −1.3 kcal mol^{-1}). In contrast, TRZS exhibits more potent interactions, especially with Arg77, forming two strong hydrogen bonds one at 2.97 Å with a notable binding energy of −7.3 kcal mol^{-1}—as well as π–H interactions with Asn28 and Ala69, mimicking key features of the bound ligand. The reference ligand demonstrates the most extensive and strongest binding network, with multiple hydrogen bonds and ionic interactions, particularly with Arg77 and Asn28, reaching energies as low as −11.6 kcal mol^{-1}. Overall, TRZS shows greater similarity to the bound ligand than ACE, indicating higher potential as a UPPS inhibitor.

3. Concluding remarks

In this study, Cs/PVP nanogels were designed as delivery platforms for hydrophobic antimicrobial scaffolds to overcome solubility and bioavailability limitations. Nanoscale characterization confirmed uniform spherical morphology (TEM: 35–110 nm), hydrodynamic diameters of 180–320 nm with narrow polydispersity (DLS), and enhanced solubility with reduced aggregation signatures (UV-Vis), highlighting controlled nanoarchitecture and colloidal stability.

Biological evaluation demonstrated a marked improvement in antibacterial potency upon nanogel encapsulation. MIC assays revealed up to 64-fold potentiation against Gram-positive pathogens, with exceptional activity against MRSA and *S. epidermidis*. Mechanistic studies further showed that TRZS-nanogels inhibited DNA gyrase with an IC_{50} of 4.44 μg mL^{-1}, representing a 5.7-fold enhancement over the free compound. Importantly, antibiofilm testing confirmed significant inhibition, reaching 79% against MRSA and 69% against *P. aeruginosa*. Cytocompatibility assays demonstrated >85% fibroblast viability at therapeutic concentrations, underscoring the safety of nanogel encapsulation. Stability testing further confirmed that the nanogels retained particle size and zeta potential over one month at storage conditions.

Collectively, these findings show that Cs/PVP nanogels not only enable precise nanoscale control but also substantially enhance antibacterial potency, biofilm inhibition, and cytocompatibility. Among the tested scaffolds, TRZS-nanogels emerged as the most promising candidate, showing the strongest enzyme inhibition and antibiofilm effects. Future work will include impurity profiling, comprehensive toxicological evaluation (mutagenicity, immunotoxicity, neurotoxicity), and *in vivo* validation to support clinical translation. Overall, Cs/PVP

Table 8 Affinity energies (kcal mol^{-1}) and intermolecular bonds of the compounds mapped to bound ligands within the active sites of the DNA gyrase target (PDB 7P2N) and undecaprenyl diphosphate synthase (PDB 2E98)

Cp.	DNA gyrase	Undecaprenyl diphosphate synthase
ACE	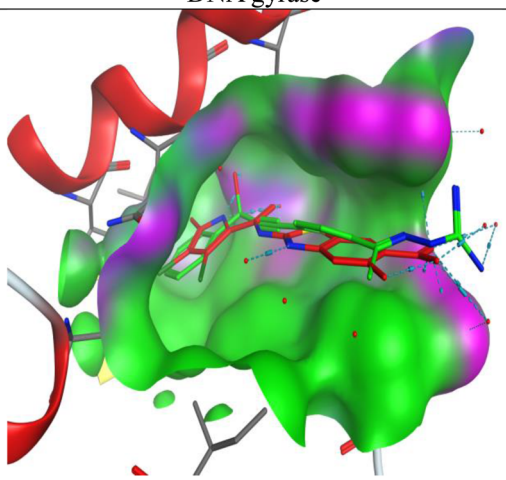 Affinity energy = −9.5	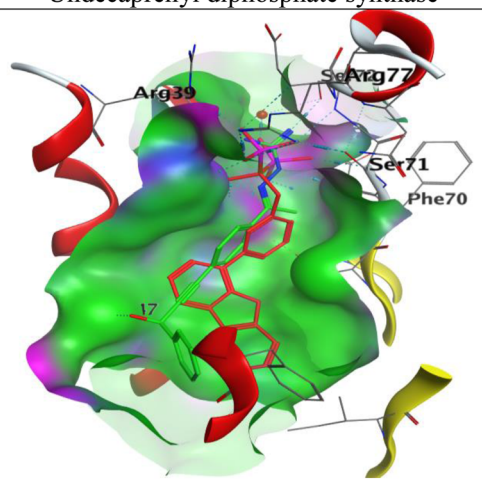 Affinity energy = −11.6
TRZS	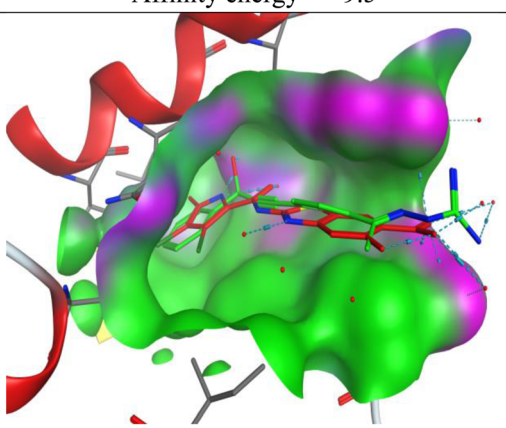 Affinity energy = −10.5	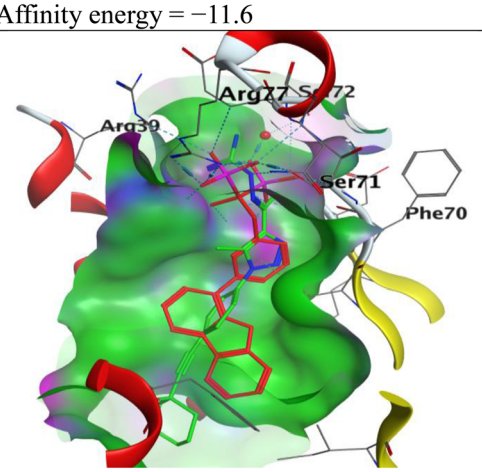 Affinity energy = −10.2

nanogels represent a highly promising next-generation antimicrobial platform for combating multidrug-resistant infections.

4. Materials and methods

The synthesis of polymer-based nanogels utilized carefully selected materials from reputable suppliers. Low molecular weight chitosan (Cs) with a degree of deacetylation ≥75% was acquired from Sigma-Aldrich (St. Louis, MO, USA). In contrast, polyvinyl pyrrolidone (PVP) with a precise molecular weight of 40 000 Da was sourced from Merck KGaA (Darmstadt, Germany). The cross-linking network was established using a combination of glutaraldehyde solution (GA, 25% w/v in H_2O, analytical grade), ammonium persulfate (APS, ≥98% purity), and *N*,*N*′-methylenebisacrylamide (MBA, 99.5% purity), all procured from Sigma-Aldrich. For pH adjustments and solvent preparations, glacial acetic acid (≥99.7% purity), sodium hydroxide pellets (NaOH, reagent grade), and concentrated hydrochloric acid (HCl, 37% v/v) were obtained from Fisher Scientific (Hampton, NH, USA).

4.1. Preparation of chitosan/PVP (Cs/PVP) nanogel

The Cs/PVP nanogel synthesis followed a modified cross-linking approach with precisely controlled reaction parameters. A chitosan solution was prepared by dissolving 0.125 g of Cs in 25 mL of 1.2% (v/v) aqueous acetic acid solution. This dissolution process was conducted under continuous magnetic stirring at 650 rpm for 2.5 hours at 25 ± 0.5 °C to ensure complete polymer solubilization. The resultant solution exhibited a viscosity of approximately 125 mPa s. The pH was meticulously adjusted to 5.2 ± 0.1 using freshly prepared 0.1 M NaOH solution added dropwise while monitoring with a calibrated pH meter (Mettler Toledo, accuracy ±0.01). Simultaneously, 0.575 g of PVP was dissolved in 35 mL of deionized water/DMSO (30/70)v/v in a separate three-necked round-bottom flask equipped with a reflux condenser. The PVP solution was heated to 62 ± 1 °C using a water bath with constant stirring at 525 rpm for 75

minutes, resulting in a transparent homogeneous solution with a viscosity of approximately 85 mPa s at 25 °C. The polymer blending process involved careful addition of the chitosan solution to the PVP solution at a controlled rate of 0.4 mL min^{-1} using a calibrated peristaltic pump (Watson–Marlow 120S). The addition was performed under vigorous stirring at 825 rpm using a Teflon-coated magnetic stir bar (40 mm × 8 mm) to promote uniform distribution of polymer chains. The mixture was maintained at 30 ± 1 °C for 90 minutes to facilitate polymer–polymer interactions through hydrogen bonding and electrostatic forces. This pre-gelation mixture demonstrated a pH of 5.4, indicating a stable colloidal system. The cross-linking process was subsequently initiated by introducing 0.024 g of APS (dissolved in 1.25 mL deionized water) as a radical initiator, followed by sequential addition of 0.0065 g of MBA (dissolved in 0.75 mL of 10% v/v ethanol solution) and 62.5 μL of GA at 5-minute intervals. The reaction vessel was purged with high-purity nitrogen gas (99.999%) for 15 minutes prior to and continuously during the cross-linking process to ensure an oxygen-free environment, preventing premature termination of the free radical polymerization. The cross-linking reaction proceeded at 72 ± 0.5 °C for 135 minutes with controlled stirring at 320 rpm, monitored using a digital overhead stirrer (IKA RW20) to prevent mechanical degradation of the forming nanogel network. Purification of the synthesized nanogel employed a two-stage approach to ensure complete removal of unreacted components and potential toxicants. The crude nanogel suspension was initially subjected to extensive dialysis using a regenerated cellulose membrane (MWCO 12–14 kDa, Spectrum Laboratories) against 4 L of deionized water for 60 hours at 4 °C. The dialysis medium was replaced every 4 hours for the first 24 hours and subsequently every 8 hours, with conductivity measurements performed to confirm the removal of ionic species (final conductivity < 10 μS cm^{-1}). Following dialysis, the nanogel suspension underwent differential centrifugation at 5250 rpm for 18 minutes at 10 °C using a refrigerated centrifuge (Eppendorf 5804R). The supernatant was discarded, and the sediment was redispersed in a 20% v/v ethanol–water mixture, followed by two additional wash cycles with 10% v/v ethanol and finally with pure deionized water. The purified Cs/PVP nanogel, exhibiting a solid content of 4.8% w/v and an average hydrodynamic diameter of 185 ± 12 nm (PDI 0.176), was stored in sterile borosilicate glass containers at 4 ± 1 °C under nitrogen atmosphere to prevent oxidative degradation before drug loading experiments.

4.2. Drug loading into Cs/PVP nanogel

The drug incorporation methodology was optimized for each compound based on its physicochemical properties. For the three selected compounds, TRZS, TRZO, and ACE; individual stock solutions were prepared at a concentration of 400 ppm in 10 mL solvent volumes (DMSO). At a concentration of 400 ppm in 10 mL of nanogel suspension. For drug solution preparation, 4 mg of each drug compounds was dissolved in 10 mL of nanogel under sonication (40 kHz, 30 minutes, 25 °C) to ensure complete solubilization, particularly for hydrophobic drugs, the solutions were filtered through 0.22 μm PTFE syringe filters to remove any potential particulate contaminants before loading. The drug loading procedure involved precise volume control and environmental conditions to maximize entrapment efficiency. Exactly 12.5 mL of Cs/PVP nanogel suspension (5.5 mg mL^{-1}) was transferred to a 50 mL jacketed glass reactor maintained at 22 ± 0.5 °C using a circulating water bath. The suspension was equilibrated under moderate magnetic stirring at 425 rpm for 15 minutes before drug addition. Each drug solution was introduced into the nanogel suspension *via* a programmable syringe pump at a controlled rate of 0.85 mL min^{-1}. The needle tip was positioned 5 mm beneath the liquid surface to minimize surface tension effects. Following complete addition, the stirring speed was increased to 475 rpm, and the mixture was maintained for 3.5 hours to facilitate drug diffusion and physical entrapment within the polymer network. The pH was monitored and maintained at 6.0 ± 0.2 for optimal electrostatic interactions between the drugs and polymer chains. Post-loading, the formulation underwent gentle sonication (15 minutes, 25% amplitude, pulsed mode: 5 s on/2 s off) in an ice bath to ensure uniform drug distribution while preventing thermal degradation.

4.3. Characterization of nanogels

The physicochemical and structural properties of the synthesized drug-loaded Cs/PVP nanogel systems were comprehensively evaluated using a complementary suite of analytical techniques. UV-Visible spectrophotometric analysis was conducted on an Agilent Cary 60 spectrophotometer equipped with a xenon flash lamp and dual silicon diode detectors.

Particle size distribution, polydispersity, and surface charge characteristics were meticulously determined using a Malvern Zetasizer Nano ZS90 equipped with a 4 mW He–Ne laser (λ = 633 nm) and an avalanche photodiode detector at a fixed backscattering angle of 173°. Dynamic light scattering measurements were performed in triplicate at 25 °C after equilibration for 120 seconds, with each measurement comprising 12 runs of 15 seconds duration. Samples were prepared by diluting the nanogel suspensions (1 : 40) in filtered (0.22 μm) ultrapure water adjusted to pH 5.5 to achieve an optimal attenuator setting of 6–8 and a 200–300 kcps count rate. High-resolution morphological characterization was performed using a JEOL JEM-2100F transmission electron microscope operating at an accelerating voltage of 200 kV with a point resolution of 0.19 nm. Nanogel suspensions were diluted to 0.01% w/v and deposited onto carbon-coated copper grids (400 mesh).

4.4. Chemistry of compounds

The supplementary material contains all details of the synthetic procedures and spectroscopic characterizations (Table S1 and Fig. S1–S7).

4.5. Biological screening

4.5.1. Determination of *in vitro* antimicrobial activity. The primary screening was carried out using the agar disc-diffusion

method.[51] Sterile paper discs (8 mm diameter) were dipped in the designed synthesized compound solution, dissolved in dimethyl sulfoxide, to achieve a specific concentration of 200 μg per disc. The antibacterial ampicillin and ciprofloxacin were used as reference antimicrobial agents. The discs were dropped on Müller–Hinton agar medium plates. The plates were previously inoculated separately with a panel of ten standard strains of ten different Gram-positive/negative bacterial strains were determined (*E. coli* ATCC 25922, *A. baumannii* ATCC 17978, *K. pneumonia* ATCC 700603, *P. aeruginosa* ATCC 25668, *P. mirabilis* ATCC 29906, *S. aureus* ATCC 43300 MRSA, *S. spidermidis* ATCC 12228, *B. subtilis* ATCC 6633, *Micrococcus luteus* ATCC 9341, and *E. feacalis* ATCC 29212). The plates were incubated at 37 °C, and the diameter of the growth inhibition zones were measured after 24 hours in case of bacteria and at 25 °C for 48 hours in case of fungi. The Minimal inhibitory concentrations (MIC) for the free compounds and nanogels against the same microorganisms used in the primary screening were carried out using the microdilution susceptibility method in Müller–Hinton Broth.[52,53] The tested and the reference compounds were dissolved in DMSO at a concentration of 64 μg mL^{-1}. The two-fold serial dilutions of the solution were prepared. The microorganism suspensions at 106 CFU mL^{-1} (colony forming unit per ml) concentrations were inoculated into the corresponding wells.[54] The MIC values were determined as the lowest concentration that inhibited the growth of the microorganism.[55] All results are mean values from at least three experiments.

4.5.2. MTT cytotoxicity evaluation. Cell viability following exposure to the synthetic compounds was estimated by MTT reduction assay.[56,57] All detailed experiments are illustrated in the SI.

4.5.3. Antibiofilm screening. The biofilm inhibitory activity of selected potent analogs at a concentration of the corresponding MICs for each compound was assessed against highly biofilm-forming Methicillin-resistant *Staphylococcus aureus* (MRSA) and *Pseudomonas aeruginosa.* The biofilm assay was carried out at the Department of Microbiology, Faculty of Pharmacy, Al-Azhar University, Cairo. See detailed methodology in supporting materials.

4.5.4. Biofilm clearance assay. The biofilm-breaking assay is a vital technique for evaluating the potential of compounds to disrupt established bacterial biofilms. Biofilms are resilient bacterial communities that can cause persistent infections and are challenging to treat due to their resistance to antibiotics. The assay typically involves allowing bacteria to form biofilms under controlled conditions, treating these biofilms with the test compounds, and then assessing the extent of biofilm disruption. Common methods for assessing disruption include crystal violet staining followed by spectrophotometric measurement, confocal laser scanning microscopy (CLSM) to visualize changes in biofilm structure, and viable cell counting to determine the number of remaining bacteria. Recent studies have shown that enzymatic approaches, such as the use of glycosidases, proteases, and deoxyribonucleases, can effectively disrupt biofilms by degrading the extracellular polymeric substance (EPS) matrix. Additionally, physical methods like ultrasound have been explored for their ability to enhance biofilm disruption.[44,58,59] These methods are crucial for developing new therapeutic strategies against biofilm-associated infections.

4.5.5. Time-killing assay. A time killing assay was performed to ascertain the activity of the phenylpyrazole compounds against MRSA, following a protocol outlined previously.[28,42] Log-phase cultures of MRSA ATCC 43300 (OD600 $\approx$ 1.00) were diluted to a final density of 2.97×10^6 CFU mL^{-1} and subjected to the test compounds at concentrations of 2–4 times their minimum inhibitory concentration (MIC), in triplicate, with Tryptic Soy Broth as the medium. At time intervals (0, 4, 6, 8, 10, 12, and 24 hours) during incubation at 37 °C, 100 μL samples were withdrawn, serially diluted in phosphate-buffered saline (PBS), and plated onto Tryptic Soy Agar. The plates were incubated at 37 °C for 18–20 hours, after which viable bacterial counts (CFU mL^{-1}) were determined. Optical density readings at 600 nm (OD600) were plotted against time (0–24 h) to monitor bacterial growth or reduction over time.

4.5.6. *E. coli* DNA gyrase supercoiling assay. The *E. coli* DNA gyrase supercoiling assay was performed at the Tissue Culture Unit, VACSERA, Giza, Egypt, using (TopoGEN kit# TG2000G-1KIT). A detailed methodology according to the Kit manufacturer.

4.5.7. Molecular docking. The target compounds ACE, TRZS and TRZO were docked into both active sites of the crystal structures of DNA Gyrase B in complex with benzothiazole (PDB: 7P2N)[60] and Undecaprenyl diphosphate synthase in complex with farnesyl pyrophosphate (PDB: 2E98)[61] target. The re-docking studies were performed for the crystal structures as a validation method. All detailed methodology was discussed in the SI materials.

Conflicts of interest

The authors declare no conflict of interest.

Data availability

The data supporting this article have been included in the main manuscript and supplementary information (SI). Supplementary information is available. See DOI: **https://doi.org/10.1039/d5ra05150a**.

Acknowledgements

The authors extend their appreciation to the Deanship of Research and Graduate Studies at King Khalid University for funding this work through Large Research Project under grant number "RGP2/602/46".

References

1 K. El-Gamal, F. Sherbiny, A. El-Morsi, H. Abu-El-khair, I. Eissa and M. El-Sebaei, Design, synthesis and antimicrobial evaluation of some novel quinoline derivatives, *Pharm. Pharmacol. Int. J.*, 2015, **2**(5), 165–177.

2 M. Elsebaei, A. A. Nasser, S. F. Hammad and A. S. Mayhoub, Synthesis Of Some New Pyrazole Derivatives As Antibacterial Agents, *Al-Azhar J. Pharm. Sci.*, 2025, **70**(2), 120–138.
3 J. M. Schierholz and J. Beuth, Implant infections: a haven for opportunistic bacteria, *J. Hosp. Infect.*, 2001, **49**(2), 87–93.
4 A. Algburi, N. Comito, D. Kashtanov, L. M. T. Dicks and M. L. Chikindas, Control of Biofilm Formation: Antibiotics and Beyond, *Appl. Environ. Microbiol.*, 2017, **83**(3), e00165.
5 L. Wang, C. Hu and L. Shao, The antimicrobial activity of nanoparticles: present situation and prospects for the future, *Int. J. Nanomed.*, 2017, **12**, 1227–1249.
6 I. Eid, M. M. Elsebaei, H. Mohammad, M. Hagras, C. E. Peters, Y. A. Hegazy, *et al.*, Arylthiazole antibiotics targeting intracellular methicillin-resistant Staphylococcus aureus (MRSA) that interfere with bacterial cell wall synthesis, *Eur. J. Med. Chem.*, 2017, **139**, 665–673.
7 F. F. Albelwi, A. A. Sheikh, M. R. Aouad, H. A. Neyaz, M. M. Khalifa, A. A. Awaji, *et al.*, Discovery of potent anticancer tricarboxamide analogs linked to 1,2,3-triazole, promoting EGFR and VEGFR downregulation, *New J. Chem.*, 2025, **49**(23), 9858–9873.
8 P. Budeli, R. C. Moropeng, L. Mpenyana-Monyatsi and M. N. B. Momba, Inhibition of biofilm formation on the surface of water storage containers using biosand zeolite silver-impregnated clay granular and silver impregnated porous pot filtration systems, *PLoS One*, 2018, **13**(4), e0194715.
9 A. Hammad, N. S. Abutaleb, M. M. Elsebaei, A. B. Norvil, M. Alswah, A. O. Ali, *et al.*, From phenylthiazoles to phenylpyrazoles: broadening the antibacterial spectrum toward carbapenem-resistant bacteria, *J. Med. Chem.*, 2019, **62**(17), 7998–8010.
10 J. K. Patra, G. Das, L. F. Fraceto, E. V. R. Campos, M. D. P. Rodriguez-Torres, L. S. Acosta-Torres, *et al.*, Nano based drug delivery systems: recent developments and future prospects, *J. Nanobiotechnol.*, 2018, **16**(1), 71.
11 G. Ferreres, K. Ivanova, I. Ivanov and T. Tzanov, Nanomaterials and Coatings for Managing Antibiotic-Resistant Biofilms, *Antibiotics*, 2023, **12**(2), 310–328.
12 A. Mancy, N. S. Abutaleb, M. M. Elsebaei, A. Y. Saad, A. Kotb, A. O. Ali, *et al.*, Balancing physicochemical properties of phenylthiazole compounds with antibacterial potency by modifying the lipophilic side chain, *ACS Infect. Dis.*, 2019, **6**(1), 80–90.
13 K. S. Soni, S. S. Desale and T. K. Bronich, Nanogels: An overview of properties, biomedical applications and obstacles to clinical translation, *J. Contr. Release*, 2016, **240**, 109–126.
14 R. Rajendran and G. Rayman, Point-of-care blood glucose testing for diabetes care in hospitalized patients: an evidence-based review, *J. Diabetes Sci. Technol.*, 2014, **8**(6), 1081–1090.
15 A. K. B. Aljohani, S. S. A. El-Hddad, M. Alsulaimany, N. A. Maghrabi, A. M. Alhammad, M. N. Aloufi, *et al.*, Design, nanogel synthesis, anti-proliferative activity and *in silico* ADMET profile of pyrazoles and pyrimidines as topo-II inhibitors and DNA intercalators, *RSC Adv.*, 2025, **15**(13), 10037–10048.
16 M. M. Elsebaie, H. T. N. El-Din, N. S. Abutaleb, A. A. Abuelkhir, H.-W. Liang, A. S. Attia, *et al.*, Exploring the structure-activity relationships of diphenylurea as an antibacterial scaffold active against methicillin-and vancomycin-resistant Staphylococcus aureus, *Eur. J. Med. Chem.*, 2022, **234**, 114204.
17 H. T. N. El-Din, M. M. Elsebaie, N. S. Abutaleb, A. M. Kotb, A. S. Attia, M. N. Seleem, *et al.*, Expanding the structure–activity relationships of alkynyl diphenylurea scaffold as promising antibacterial agents, *RSC Med. Chem.*, 2023, **14**(2), 367–377.
18 S. Malhotra-Kumar, K. Haccuria, M. Michiels, M. Ieven, C. Poyart, W. Hryniewicz, *et al.*, Current trends in rapid diagnostics for methicillin-resistant Staphylococcus aureus and glycopeptide-resistant enterococcus species, *J. Clin. Microbiol.*, 2008, **46**(5), 1577–1587.
19 M. Hagras, N. S. Abutaleb, A. O. Ali, J. A. Abdel-Aleem, M. M. Elsebaei, M. N. Seleem, *et al.*, Naphthylthiazoles: targeting multidrug-resistant and intracellular Staphylococcus aureus with biofilm disruption activity, *ACS Infect. Dis.*, 2018, **4**(12), 1679–1691.
20 Y. Hosny, N. S. Abutaleb, M. Omara, M. Alhashimi, M. M. Elsebaei, H. S. Elzahabi, *et al.*, Modifying the lipophilic part of phenylthiazole antibiotics to control their drug-likeness, *Eur. J. Med. Chem.*, 2020, **185**, 111830.
21 M. M. Elsebaei, H. Mohammad, M. Abouf, N. S. Abutaleb, Y. A. Hegazy, A. Ghiaty, *et al.*, Alkynyl-containing phenylthiazoles: Systemically active antibacterial agents effective against methicillin-resistant Staphylococcus aureus (MRSA), *Eur. J. Med. Chem.*, 2018, **148**, 195–209.
22 M. Almaghrabi, A. Musa, A. K. B. Aljohani, H. E. A. Ahmed, M. Alsulaimany, S. F. Miski, *et al.*, Introducing of novel class of pyrano[2,3-c]pyrazole-5-carbonitrile analogs with potent antimicrobial activity, DNA gyrase inhibition, and prominent pharmacokinetic and CNS toxicity profiles supported by molecular dynamic simulation, *J. Biomol. Struct. Dyn.*, 2024, **42**(18), 9529–9546.
23 M. Almaghrabi, A. Musa, A. K. B. Aljohani, H. E. A. Ahmed, M. Alsulaimany, S. F. Miski, *et al.*, Introducing of novel class of pyrano[2,3-c]pyrazole-5-carbonitrile analogs with potent antimicrobial activity, DNA gyrase inhibition, and prominent pharmacokinetic and CNS toxicity profiles supported by molecular dynamic simulation, *J. Biomol. Struct. Dyn.*, 2023, 1–18.
24 A. M. Malebari, H. E. A. Ahmed, S. K. Ihmaid, A. M. Omar, Y. A. Muhammad, S. S. Althagfan, *et al.*, Exploring the dual effect of novel 1,4-diarylpyranopyrazoles as antiviral and anti-inflammatory for the management of SARS-CoV-2 and associated inflammatory symptoms, *Bioorg. Chem.*, 2023, **130**, 106255.
25 M. M. Elsebaei, N. S. Abutaleb, A. A. Mahgoub, D. Li, M. Hagras, H. Mohammad, *et al.*, Phenylthiazoles with nitrogenous side chain: An approach to overcome molecular obesity, *Eur. J. Med. Chem.*, 2019, **182**, 111593.

26 A. M. Sayed, N. S. Abutaleb, A. Kotb, H. G. Ezzat, M. N. Seleem, A. S. Mayhoub, *et al.*, Arylpyrazole as selective anti-enterococci; synthesis and biological evaluation of novel derivatives for their antimicrobial efficacy, *J. Heterocycl. Chem.*, 2023, **60**(1), 134–144.

27 A. A. Abuelkhir, Y. I. Nagy, T. Gamal, A. M. Abdelhalim, A. S. Attia, A. S. Mayhoub, *et al.*, Small Molecule Alkynyl-Phenylaminoguanidines: A New Weapon Against Multi-Drug Resistant Bacteria, *ChemistrySelect*, 2025, **10**(4), e202404320.

28 M. M. Elsebaei, H. G. Ezzat, A. M. Helal, M. H. El-Shershaby, M. S. Abdulrahman, M. Alsedawy, *et al.*, Rational design and synthesis of novel phenyltriazole derivatives targeting MRSA cell wall biosynthesis, *RSC Adv.*, 2024, **14**(54), 39977–39994.

29 M. Omara, M. Hagras, M. M. Elsebaie, N. S. Abutaleb, H. T. N. El-Din, M. O. Mekhail, *et al.*, Exploring novel aryl/heteroaryl-isosteres of phenylthiazole against multidrug-resistant bacteria, *RSC Adv.*, 2023, **13**(29), 19695–19709.

30 M. M. Elsebaei, H. Mohammad, A. Samir, N. S. Abutaleb, A. B. Norvil, A. R. Michie, *et al.*, Lipophilic efficient phenylthiazoles with potent undecaprenyl pyrophosphatase inhibitory activity, *Eur. J. Med. Chem.*, 2019, **175**, 49–62.

31 I. G. Shahin, K. O. Mohamed, A. T. Taher, M. M. Elsebaei, A. S. Mayhoub, A. E. Kassab, *et al.*, New Phenylthiazoles: Design, Synthesis, and Biological Evaluation as Antibacterial, Antifungal, and Anti-COVID-19 Candidates, *Chem. Biodiversity*, 2023, **20**(11), e202301143.

32 M. Hagras, N. S. Abutaleb, N. M. Elhosseiny, T. M. Abdelghany, M. Omara, M. M. Elsebaei, *et al.*, Development of biphenylthiazoles exhibiting improved pharmacokinetics and potent activity against intracellular Staphylococcus aureus, *ACS Infect. Dis.*, 2020, **6**(11), 2887–2900.

33 A. M. Helal, A. M. Sayed, M. Omara, M. M. Elsebaei and A. S. Mayhoub, Peptidoglycan pathways: there are still more, *RSC Adv.*, 2019, **9**(48), 28171–28185.

34 H. E. Ahmed, M. A. El-Nassag, A. H. Hassan, H. M. Mohamed, A. H. Halawa and R. M. Okasha, Developing lipophilic aromatic halogenated fused systems with specific ring orientations, leading to potent anticancer analogs and targeting the c-Src Kinase enzyme, *J. Enzyme Inhib. Med. Chem.*, 2019, **1186**, 212–223.

35 H. E. Ahmed, S. K. Ihmaid, A. M. Omar, A. M. Shehata, H. S. Rateb and M. F. Zayed, Design, synthesis, molecular docking of new lipophilic acetamide derivatives affording potential anticancer and antimicrobial agents, *Bioorg. Chem.*, 2018, **76**, 332–342.

36 H. E. A. Ahmed, A. Amer, S. A. Senior, S. Ihmaid, M. Almalghrabi and A.-M. E. Massry, Extensive Study of DFT-Quantum Calculations Based QSAR Modeling of Fused 1,2,4-Triazine Derivatives Revealed Potent CYP1A1 Inhibitors, *J. Comput. Biophys. Chem.*, 2022, **21**, 741–758.

37 H. E. A. Ahmed, M. A. A. El-Nassag, A. H. Hassan, H. M. Mohamed, A. H. Halawa, R. M. Okasha, *et al.*, Developing lipophilic aromatic halogenated fused systems with specific ring orientations, leading to potent anticancer analogs and targeting the c-Src Kinase enzyme, *J. Mol. Struct.*, 2019, **1186**, 212–223.

38 L. M. Al-Harbi, E. A. Al-Harbi, R. M. Okasha, R. A. El-Eisawy, M. A. A. El-Nassag, H. M. Mohamed, *et al.*, Discovery of benzochromene derivatives first example with dual cytotoxic activity against the resistant cancer cell MCF-7/ADR and inhibitory effect of the P-glycoprotein expression levels, *J. Enzyme Inhib. Med. Chem.*, 2023, **38**(1), 2155814.

39 A. Aljuhani, H. E. A. Ahmed, S. K. Ihmaid, A. M. Omar, S. S. Althagfan, Y. M. Alahmadi, *et al.*, In vitro and computational investigations of novel synthetic carboxamide-linked pyridopyrrolopyrimidines with potent activity as SARS-CoV-2-M(Pro) inhibitors, *RSC Adv.*, 2022, **12**(41), 26895–26907.

40 H.-S. Cui, Z.-R. Wu, X.-Y. Shi, G.-Q. Dong, S.-N. Ding, N. Bao, *et al.*, CS/PVP Hydrogel-Based Nanocapillary for Monitoring Bacterial Growth and Rapid Antibiotic Susceptibility Testing, *ACS Sens.*, 2024, **9**(7), 3540–3548.

41 B. Almohaywi, H. E. A. Ahmed, A. Kotb, A. Ashraf, M. Alsedawy, E. L. S. E. Habib, *et al.*, Triazole-functionalized compounds as promising antifungal agents: Synthesis, biological evaluation, and mechanistic insights, *Naunyn-Schmiedeberg's Arch. Pharmacol.*, 2025, 1–21.

42 M. M. Elsebaei, H. G. Ezzat, A. M. Helal, M. H. El-Shershaby, M. S. Abdulrahman, M. Alsedawy, *et al.*, Rational design and synthesis of novel phenyltriazole derivatives targeting MRSA cell wall biosynthesis, *RSC Adv.*, 2024, **14**(54), 39977–39994.

43 H. E. A. Ahmed, S. K. Ihmaid, A. M. Omar, A. M. Shehata, H. S. Rateb, M. F. Zayed, *et al.*, Design, synthesis, molecular docking of new lipophilic acetamide derivatives affording potential anticancer and antimicrobial agents, *Bioorg. Chem.*, 2018, **76**, 332–342.

44 A. A. Awaji, W. A. Z. El Zaloa, M. A. Seleem, M. Alswah, M. M. Elsebaei, A. H. Bayoumi, *et al.*, N-and s-substituted Pyrazolopyrimidines: A promising new class of potent c-Src kinase inhibitors with prominent antitumor activity, *Bioorg. Chem.*, 2024, **145**, 107228.

45 D. Keskin, G. Zu, A. M. Forson, L. Tromp, J. Sjollema and P. van Rijn, Nanogels: A novel approach in antimicrobial delivery systems and antimicrobial coatings, *Bioact. Mater.*, 2021, **6**(10), 3634–3657.

46 H. Le, C. Karakasyan, T. Jouenne, D. Le Cerf and E. Dé, Application of Polymeric Nanocarriers for Enhancing the Bioavailability of Antibiotics at the Target Site and Overcoming Antimicrobial Resistance, *Appl. Sci.*, 2021, **11**(22), 1–34.

47 Y. Xie, H. Liu, Z. Teng, J. Ma and G. Liu, Nanomaterial-enabled anti-biofilm strategies: new opportunities for treatment of bacterial infections, *Nanoscale*, 2025, **17**(10), 5605–5628.

48 Y. Gao, Q. Cao, Y. Xiao, Y. Wu, L. Ding, H. Huang, *et al.*, The progress and future of the treatment of Candida albicans infections based on nanotechnology, *J. Nanobiotechnol.*, 2024, **22**(1), 568.

49 A. Hussien, A. Musa, H. T. N. El-Din, A. M. Helal, Y. I. Nagy, H. G. Ezzat, *et al.*, Phenyltriazole-based sulfonamides: novel

dual-target agents against MRSA biofilms and resistant pathogens, *RSC Adv.*, 2025, **15**(22), 17186–17202.

50 B. Almohaywi, H. E. Ahmed, A. Kotb, A. Ashraf, M. Alsedawy, E.-S. E. Habib, *et al.*, Triazole-functionalized compounds as promising antifungal agents: Synthesis, biological evaluation, and mechanistic insights, *Naunyn-Schmiedeberg's Arch. Pharmacol.*, 2025, 1–21.

51 P. Wayne, *Performance Standards For Antimicrobial Susceptibility Testing*, Clinical and laboratory standards institute, 2011.

52 P. Murray, E. J. Baron, M. Pfaller, F. Tenover and R. H. Yolken, *Manual of Clinical Microbiology*, ASM Press, Washington, DC, 1999.

53 I. Wiegand, K. Hilpert and R. E. Hancock, Agar and broth dilution methods to determine the minimal inhibitory concentration (MIC) of antimicrobial substances, *Nat. Protoc.*, 2008, **3**(2), 163–175.

54 N. Rezki, S. A. Al-Sodies, H. E. A. Ahmed, S. Ihmaid, M. Messali, S. Ahmed, *et al.*, A novel dicationic ionic liquids encompassing pyridinium hydrazone-phenoxy conjugates as antimicrobial agents targeting diverse high resistant microbial strains, *J. Mol. Liq.*, 2019, **284**, 431–444.

55 I. Wiegand, K. Hilpert and R. E. Hancock, Agar and broth dilution methods to determine the minimal inhibitory concentration (MIC) of antimicrobial substances, *Nat. Protoc.*, 2008, **3**(2), 163–175.

56 T. Mosmann, Rapid colorimetric assay for cellular growth and survival: application to proliferation and cytotoxicity assays, *J. Immunol. Methods*, 1983, **65**(1–2), 55–63.

57 F. Demirci and K. H. C. Başer, Bioassay Techniques for Drug Development By Atta-ur-Rahman, M. Iqbal Choudhary (HEJRIC, University of Karachi, Pakistan), William J. Thomsen (Areana Pharmaceuticals, San Diego, CA). Harwood Academic Publishers, Amsterdam, The Netherlands. 2001. xii + 223 pp. 15.5 × 23.5 cm. $79.00. ISBN 90-5823-051-1, *J. Nat. Prod.*, 2002, **65**(7), 1086–1087.

58 S. Wang, A. P. Breslawec, C. Li and M. B. Poulin, A Colorimetric Assay to Enable High-Throughput Identification of Biofilm Exopolysaccharide-Hydrolyzing Enzymes, *Chemistry*, 2020, **26**(47), 10719–10723.

59 M. Elsebaei, A. Y. Saad, A. S. Mayhoub and K. A. Ali, Synthesis Of New Chloroquine Derivatives For Biological Studies, *Al-Azhar J. Pharm. Sci.*, 2024, **70**(2), 103–119.

60 M. Sterle, M. Durcik, C. E. M. Stevenson, S. R. Henderson, P. E. Szili, M. Czikkely, *et al.*, Exploring the 5-Substituted 2-Aminobenzothiazole-Based DNA Gyrase B Inhibitors Active against ESKAPE Pathogens, *ACS Omega*, 2023, **8**(27), 24387–24395.

61 M. Jukič, K. Rožman, M. Sova, H. Barreteau and S. Gobec, Anthranilic Acid Inhibitors of Undecaprenyl Pyrophosphate Synthase (UppS), an Essential Enzyme for Bacterial Cell Wall Biosynthesis, *Front. Microbiol.*, 2018, **9**, 3322.